Economic Geology
Vol. 92, 1997, pp. 601–622

$^{40}Ar/^{39}Ar$ Dating and Mineral Paragenesis for Carlin-Type Gold Deposits along the Getchell Trend, Nevada: Evidence for Cretaceous and Tertiary Gold Mineralization

JOHN A. GROFF,

Department of Earth and Environmental Sciences, New Mexico Institute of Mining and Technology, 801 Leroy, Socorro, New Mexico 87801

MATTHEW T. HEIZLER,[†]

New Mexico Bureau of Mines and Mineral Resources, New Mexico Institute of Mining and Technology, 801 Leroy, Socorro, New Mexico 87801

WILLIAM C. MCINTOSH,

Department of Earth and Environmental Sciences and New Mexico Bureau of Mines and Mineral Resources, New Mexico Institute of Mining and Technology, 801 Leroy, Socorro, New Mexico 87801

AND DAVID I. NORMAN

Department of Earth and Environmental Sciences, New Mexico Institute of Mining and Technology, 801 Leroy, Socorro, New Mexico 87801

Abstract

The orebodies at the Getchell and Twin Creeks mines were studied through mineral paragenesis, geologic relationships, and $^{40}Ar/^{39}Ar$ dating. Mineral paragenetic relationships are based on observations made during the logging of 18,000 m of drill cuttings and core and crosscutting relationships recognized in the field and Main pit at the Getchell mine. Ages for igneous and mineralizing events were determined through $^{40}Ar/^{39}Ar$ incremental heating analyses of 15 samples of biotite, K feldspar, sericite, and vein adularia. A thermal history for the area was also developed using K feldspar multiple diffusion domain results and age determinations on cogenetic minerals, which have different argon closure temperatures.

Mineral paragenetic relationships and $^{40}Ar/^{39}Ar$ dating at the Getchell and Twin Creeks deposits document that gold mineralization occurred in five stages between 95 and 42 Ma.

Stage 1 pyrrhotite-quartz-arsenopyrite-chalcopyrite-biotite gold mineralization in skarn is associated with 95 Ma dacite dikes and granodiorite plugs. Stage 2 chalcopyrite-sphalerite-galena-pyrite-arsenopyrite ± gold and silver mineralization in skarn is related to the 92 Ma Osgood Mountains stock. Secondary K feldspar and sericite in stage 3 quartz-pyrite-kaolinite-gold mineralization formed at 83 Ma and are not related to 95 or 92 Ma igneous activity. Stage 4 low-grade quartz-pyrite-gold mineralization formed at about 75 Ma, in the matrix of a breccia pipe that cuts 83 Ma silicic and argillic ores. Adularia intergrown with stibnite-orpiment-pyrite-quartz-gold ± realgar mineralization yields precise $^{40}Ar/^{39}Ar$ plateau ages of 42.11 ± 0.43 and 41.90 ± 0.25 Ma for stage 5.

This study documents the temporal complexity of mineralization and igneous activity at the Getchell and Twin Creeks deposits. Minor gold in skarn-type mineralization (stages 1 and 2) associated with 95 and 92 Ma igneous intrusions preceded and was not genetically related to Carlin-type gold mineralization (stages 3 and 5). The Carlin-type deposits at Getchell and Twin Creeks therefore represent a composite orebody formed by the overprinting of 83 Ma stage 3 quartz-pyrite-gold by 42 Ma stage 5 orpiment-stibnite-pyrite-gold mineralization.

Introduction

CARLIN-TYPE gold deposits are a major economic resource, but due to a poor understanding of the timing of gold mineralization, a detailed genetic model for these deposits has yet to be developed. Carlin-type deposits in Nevada are located in three gold belts known as the Carlin trend, the Battle Mountain-Eureka trend, and the Getchell trend. Although defined by linear alignments of gold deposits, these trends are thought to represent major crustal structures, based on the distribution of igneous intrusions and coincidence with fault zones and geophysical discontinuities (Shawe, 1991). In this paper we use the term "Carlin-type gold deposit" to be synonymous with sediment-hosted gold deposit (Berger, 1986, p. 175). As will be discussed in the mineral paragenesis portion of this manuscript, the Getchell and Twin Creeks deposits share the following characteristics with deposits on the Carlin trend: (1) micron to submicron gold in pyrite, (2) a trace element signature of Au-As-Hg-Sb-Tl and lack of Cu-Pb-Zn, (3) the mineral assemblage of quartz-orpiment-realgar-stibnite, (4) a host-rock package with carbonaceous, thinly bedded limestone, shale, and chert, and (5) wall-rock alteration typified by carbonate dissolution followed by silicification and argillization (Bagby and Berger, 1985).

The main purpose of this paper is to report $^{40}Ar/^{39}Ar$ dates of samples that are closely tied to mineral paragenesis and geologic relationships of the Getchell and Twin Creeks deposits. Included in this study are samples of primary biotite, hornblende, and K feldspar from igneous intrusions and hydrothermal biotite, sericite, K feldspar, and vein adularia from gold-bearing rocks.

Regional Geology

The tectonic evolution of northern Nevada is characterized by multiple orogenies and thrusting events, igneous activity, and basin-and range deformation (Hotz and Wilden, 1964;

[†] Corresponding author: email, bureau@gis.nmt.edu

0361-0128/97/1927/601-22$6.00

Roberts, 1964; Erickson and Marsh, 1974; Madrid, 1987). In the area of the Getchell and Twin Creeks deposits (Fig. 1a) folding on a regional scale accompanied thrusting during the Late Devonian to Middle Pennsylvanian (Antler orogeny). A second thrusting event occurred during the Permian to Early Triassic (Sonoma orogeny) and preceded extensional tectonism and igneous activity in the Eocene. Extensional deformation and bimodal volcanism associated with basin-and range tectonism was most pronounced during the Miocene.

The Getchell and Twin Creeks deposits are located on the eastern flank of the Osgood Mountains, ~72 km northeast of Winnemucca, Nevada, where Paleozoic rocks are intruded by Cretaceous igneous bodies and locally overlain by Tertiary volcanics (Fig. 1a, b). The Paleozoic stratigraphic section at the Getchell and Twin Creeks mines includes the Cambrian Preble Formation, the Ordovician Comus and Valmy Formations, the Pennsylvanian to Permian Etchart Formation, and the Mississippian Farrell Canyon Formation (Fig. 1b). The Preble Formation consists of thin beds of interlayered limestones and carbonaceous shale (Rowell et al., 1979). The Preble Formation is conformably overlain by the Ordovician Comus Formation, a sequence of interbedded limestone, carbonaceous and calcareous shale, and some mafic volcanic rock (Berger and Taylor, 1980). The contact between the Comus and Valmy Formations is complex and represents a thrust fault. The Valmy Formation is characterized by basalt, shale, chert, quartzite, and minor limestone (Madrid, 1987). The Valmy Formation is separated from the Pennsylvanian to Permian limestone of the Etchart Formation by either a thrust fault or an angular unconformity (Roberts, 1966). A thrust fault separates thinly interbedded siltstone, chert, and limestone of the Farrell Canyon Formation from the Etchart Formation (Hotz and Wilden, 1964).

Numerous Cretaceous igneous bodies intrude the Paleozoic strata. These include the ~92 Ma Osgood Mountains granodiorite stock (Silberman et al., 1974), associated pegmatite and aplite dikes, dacite dikes compositionally similar to the granodiorite stock, and porphyritic andesite dikes (Hotz and Wilden, 1964). Intrusion of the Osgood Mountains granodiorite stock resulted in the formation of a contact metamorphic aureole that extends as much as 3 km from the stock. Metamorphism is represented by biotite-cordierite hornfels, andalusite hornfels, wollastonite-bearing calc-silicate skarn, marble, and a garnet-rich skarn at the margin of the stock. The Paleozoic section in the study area is locally overlain by 15 Ma bimodal volcanics (Madden-McGuire et al., 1991).

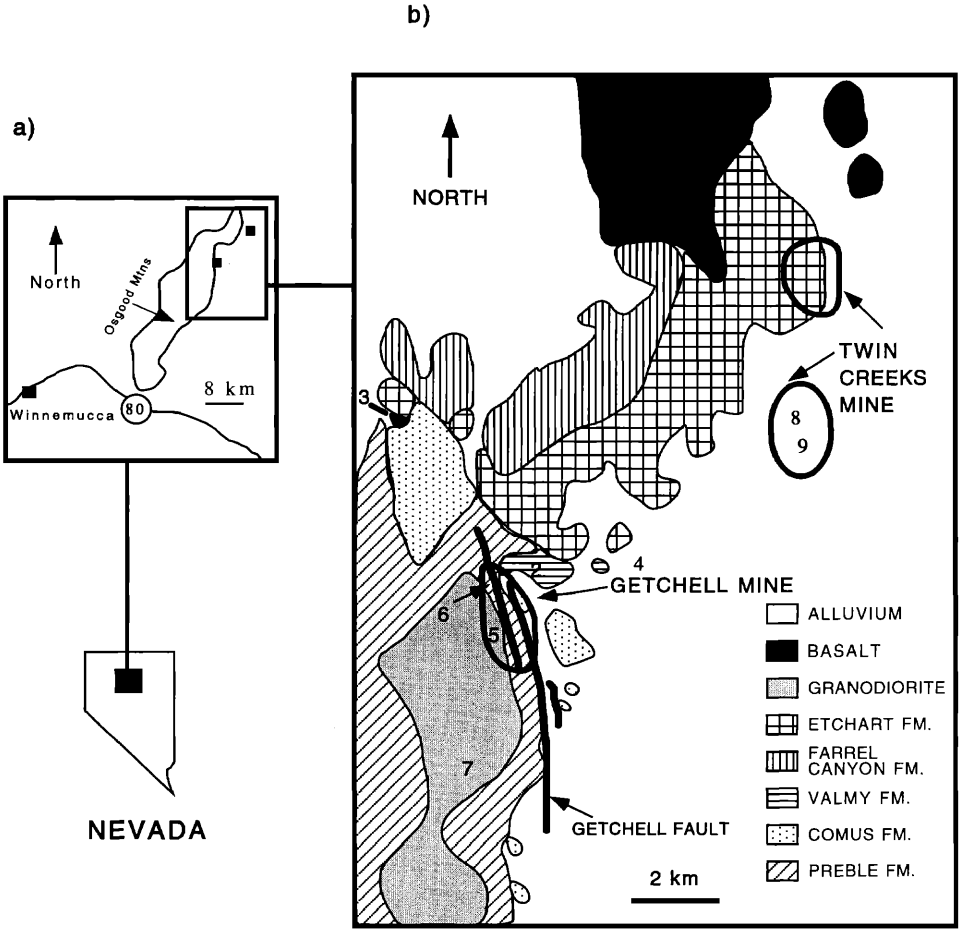

FIG. 1. Location of (a) the Getchell and Twin Creeks mines on the eastern flank of the Osgood Mountains relative to the town of Winnemucca and Interstate 80, and (b) geologic map of the northern end of the Getchell trend (after Hotz and Wilden, 1964). Numbered areas represent localities where samples for $^{40}Ar/^{39}Ar$ dating were obtained.

Problems with Dating Carlin-Type Gold Deposits

Absolute dating of gold mineralization in Carlin-type deposits has been hindered because of the fine-grained nature of the mineralization and complex mineral paragenesis. Electron microprobe studies (Bakken et al., 1989; Arehart et al., 1993a,b) indicate that micron to submicron gold is contained in arsenic-rich pyrite or encapsulated in quartz. The presence of multiple mineralizing events, all potentially gold bearing, in districts that contain Carlin-type deposits (Wrucke and Armubrustmacher, 1975; Kuehn, 1989; Shawe and Nolan, 1989; Groff and Norman, 1993) further complicates the interpretation of age dates and documentation of the age(s) of gold mineralization.

Due to the complex overprinting of mineralization and igneous activity, and the lack of datable minerals, research by past workers has resulted in multiple interpretations for the age of gold mineralization. Igneous activity in the Cretaceous, Eocene, and Miocene has been documented for the Battle Mountain-Eureka, Carlin, and Getchell trends (Silberman et al., 1974; Wrucke and Armubrustmacher, 1975; Radtke, 1985; Madden-McGuire et al., 1991; Shawe, 1991; Arehart et al., 1993b; Wallace, 1993). These high-temperature igneous and hydrothermal events could potentially cause argon loss or reset the ages of minerals that grew during gold mineralization. However, complex age spectra for minerals that may have experienced argon loss in relation to gold mineralization are difficult to interpret and yield controversial results (Arehart et al., 1993b; Ilchik, 1995). Reported ages of potassium-rich minerals that are not constrained by mineral paragenesis and only spatially related to gold mineralization have also contributed to the conflicting views regarding the timing of gold mineralization. Due to these factors the interpretation of age dates for the Getchell, Post-Betze, and Mercur mines (Silberman et al., 1974; Moore and McKee, 1983; Bettles and Lauha, 1991; Arehart et al., 1993b; Wilson and Parry, 1995) suggest that gold mineralization may have occurred sometime during the interval of 160 to 32 Ma.

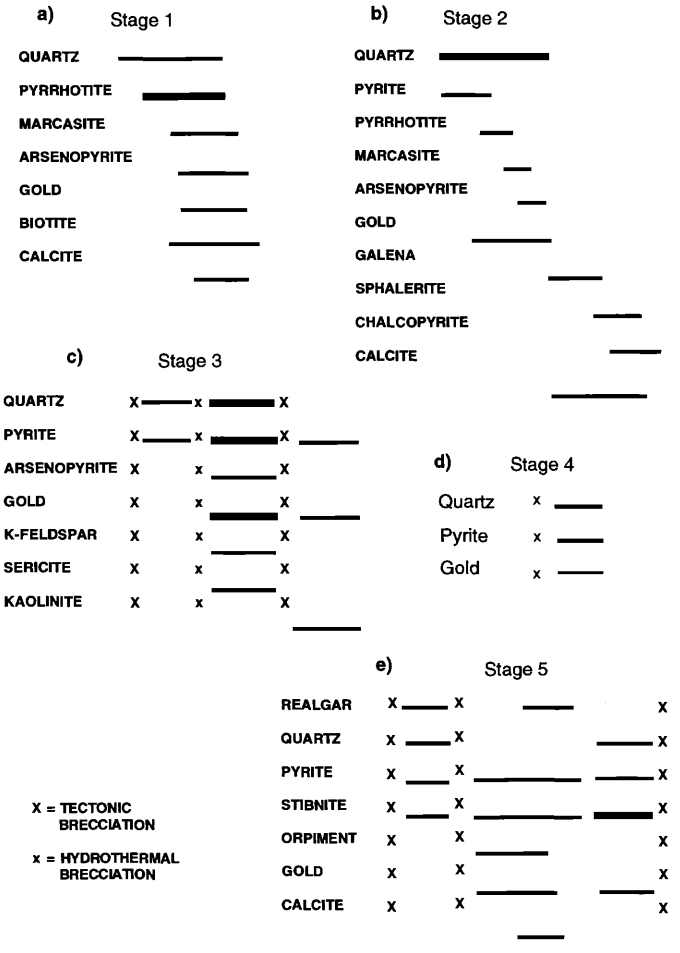

FIG. 2. Mineral paragenesis for the Getchell property representing (a) stage 1 mineralization, (b) stage 2 mineralization, (c) stage 3 mineralization, (d) stage 4 mineralization in the matrix of a breccia pipe, and (e) stage 5 mineralization. The width of the horizontal bars represent the relative importance of each mineral in the paragenetic sequence.

Mineral Paragenesis

The paragenesis of mineralization for the Getchell deposit was determined in order to provide a relative temporal framework, within which absolute ages would be determined by $^{40}Ar/^{39}Ar$ geochronology. Paragenetic relationships were determined through pit mapping, field sampling, and the logging of 18,000 m of drill cuttings and core at the Getchell mine. Field work, microscopy, and assays of mineral separates indicate that gold is associated with six mineralogically distinct assemblages (Fig. 2a-e) that are thought to represent distinct episodes of mineralization (here termed stages 1–5).

Skarn formation at the Getchell deposit predated and was associated with the emplacement of the Osgood Mountains stock. Stage 1 is represented by an extensive pyrrhotite-rich skarn that is best developed in the Preble Formation, basalt of the Valmy Formation, and Cretaceous dacite dikes (Hotz and Wilden, 1964). Pyrrhotite is volumetrically the most significant mineral in this skarn, but lesser amounts of arsenopyrite, chalcopyrite, marcasite, and biotite are present (Fig. 2a). Stage 2 is contained in the garnet-rich skarn, adjacent to the Osgood Mountains stock, and as veins that cut the stock. Chalcopyrite, sphalerite, and galena with ubiquitous pyrite and lesser amounts of arsenopyrite, marcasite, and pyrrhotite + silver characterize stage 2. Gold in stages 1 and 2 was never identified optically and is based solely on assay data. Assays of gold in small silicified pods in stages 1 and 2 skarns range from 0 to a maximum of 2.5 ppm.

The relative ages of stages 1 and 2 were determined by field relationships with ~92 Ma andesite dikes (Berger and Taylor, 1980). Stage 1 predated the emplacement of the ~92 Ma Osgood Mountains stock based on ~92 Ma andesite dikes, which are similar in composition to the stock (Hotz and Wilden, 1964; Berger and Taylor, 1980) that cuts stage 1 pyrrhotite-rich skarn (Fig. 3a). At the same locality, the andesite dikes are brecciated and healed by a siliceous matrix that contains stage 2 base metal mineralization (Fig. 3a).

Stage 3 mineralization at the Getchell deposit is contained in fault zones that cut the Osgood Mountains stock and skarn of stages 1 and 2. In the Getchell fault, blocks of stage 1 pyrrhotite-rich skarn and barren Osgood Mountains stock are bounded by fault gouge containing stage 3 mineralization. Movement along the Getchell fault is observed to offset stage 2 quartz-base metal veins prior to stage 3 mineralization.

The flow of stage 3 mineralizing fluids at the Getchell

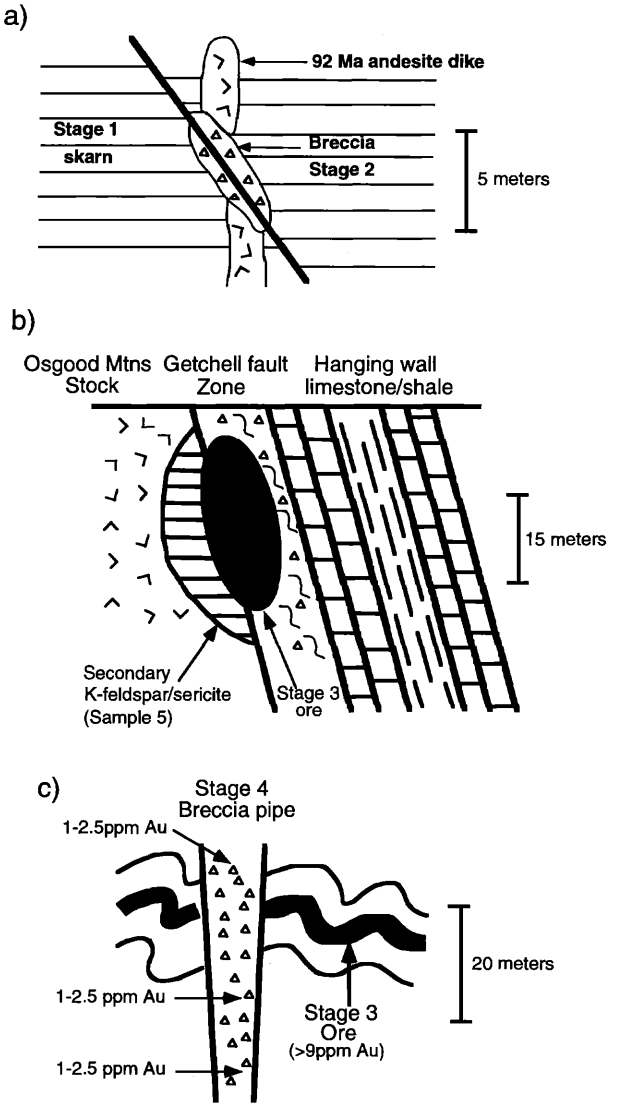

FIG. 3. Schematic diagrams showing the crosscutting relationships for (a) stages 1 and 2 relative to ~92 Ma andesite dikes, (b) potassium-rich alteration in association with stage 3 mineralization at the Getchell mine, and (c) stage 4 mineralization in a breccia pipe relative to stage 3 ores in the underground, Getchell mine. The uniform gold abundance throughout the breccia pipe suggests that stage 4 represents a discrete mineralization event rather than random mobilization of gold from stage 3 rocks during breccia pipe emplacement.

deposit was strongly influenced by the Osgood Mountains stock and skarn formation associated with stages 1 and 2. Ponding of stage 3 mineralization beneath lobes and sills of granodiorite is common and resulted in a distinct style of alteration. Granodiorite in contact with stage 3 mineralization was potassically altered as recognized by sericite replacement of biotite and secondary K feldspar replacement of plagioclase (Figs. 3b, 4). XRD analyses (not shown) confirm the optical identification of K feldspar after plagioclase from three samples of stage 3 mineralized igneous rocks. This potassium-rich phase of alteration was only identified in close proximity to stage 3 mineralization and cuts skarns that developed during stages 1 and 2. Sericitic alteration was also recognized by Arehart et al. (1993b) at the Post-Betze deposit where argillic and silicic ores overprinted the Jurassic Goldstrike stock. Skarn formation associated with stages 1 and 2 at the Getchell mine also decreased the receptivity of host rocks to stage 3 mineralization and resulted in low-grade or barren zones at the Getchell mine.

The bulk of the ore mined at the Getchell and Twin Creeks deposits consists of gold and fine-grained pyrite in association with stage 3 hydrothermal silicification and argillic alteration (Fig. 2c). Multiple episodes of silicification at the beginning of stage 3 are recognized by textural and color differences, as well as silica-healed breccias that contain clasts of silicified and quartz-veined rocks. Silicified clasts in breccias commonly contain pyrite and possibly gold; however, gold mineralization is closely associated with pyrite-rich (20–40%) quartz in the matrix of breccias (Fig. 2c).

Movement along the Getchell fault during stage 3 is based on fragments of pyritic quartz and silica-healed breccias contained in argillic ores. Gold in argillic ores is closely associated with fine-grained pyrite (Fig. 2c), which is either disseminated or occurs as distinct bands.

Stage 4 mineralization is characterized by low-grade quartz-pyrite-gold mineralization in the matrix of two breccia pipes that cut stage 3 argillic and silicic ores in the underground workings at the Getchell mine (Fig. 2d). These breccia pipes contain exotic clasts (Osgood Mountains stock, pegmatitic K feldspar, chert, siltstone, and limestone) in a matrix of auriferous pyrite (1–2.5 ppm gold) and quartz. Low-grade gold mineralization in the breccia pipes is vertically continuous, for at least 50 m, and does not represent contamination from high-grade stage 3 ores (>9 ppm) that are cut by the pipes higher in the system (Fig. 3c).

Stage 5 ores mined at the Getchell and Twin Creeks deposits are generally confined to structural zones and occur as open-space fillings, as the matrix of breccias which contain clasts of stage 3 mineralization, and as veins that crosscut stage 3. Stage 5 began with the deposition of realgar-quartz-pyrite-stibnite (Fig. 2e), and assays of these minerals do not detect gold. Tectonic brecciation separates realgar-quartz-pyrite-stibnite mineralization from orpiment-pyrite-gold mineralization. This is evidenced by breccias that have realgar-veined quartz clasts and an orpiment matrix and gouge zones that contain broken pieces of realgar and quartz which are cut by orpiment veins (Fig. 2e). Realgar-calcite-pyrite ± gold overlaps and postdates orpiment-pyrite-gold mineralization (Fig. 2e). Orpiment and realgar-calcite mineralization is generally closely associated, with realgar located along cleavage planes in orpiment, and the orpiment crystals commonly surrounded by realgar and calcite. Assays of orpiment separates indicate the association of gold (0.5–3 ppm) with orpiment, and native gold was also identified petrographically in one sample of calcite.

The youngest gold mineralizing event in stage 5 at the Getchell deposit is composed of stibnite-quartz-pyrite-gold veins or open-space fillings (Fig. 2e). Stibnite commonly occurs as coatings on realgar and calcite crystals, or more rarely as quartz-stibnite-pyrite veins that cut realgar and calcite-bearing orpiment.

Gold mineralization at the Getchell deposit was followed by the deposition of finely banded chalcedonic quartz and calcite with minor pyrite, sphalerite, and chalcopyrite. In some cases, breccias contain rounded clasts of finely banded

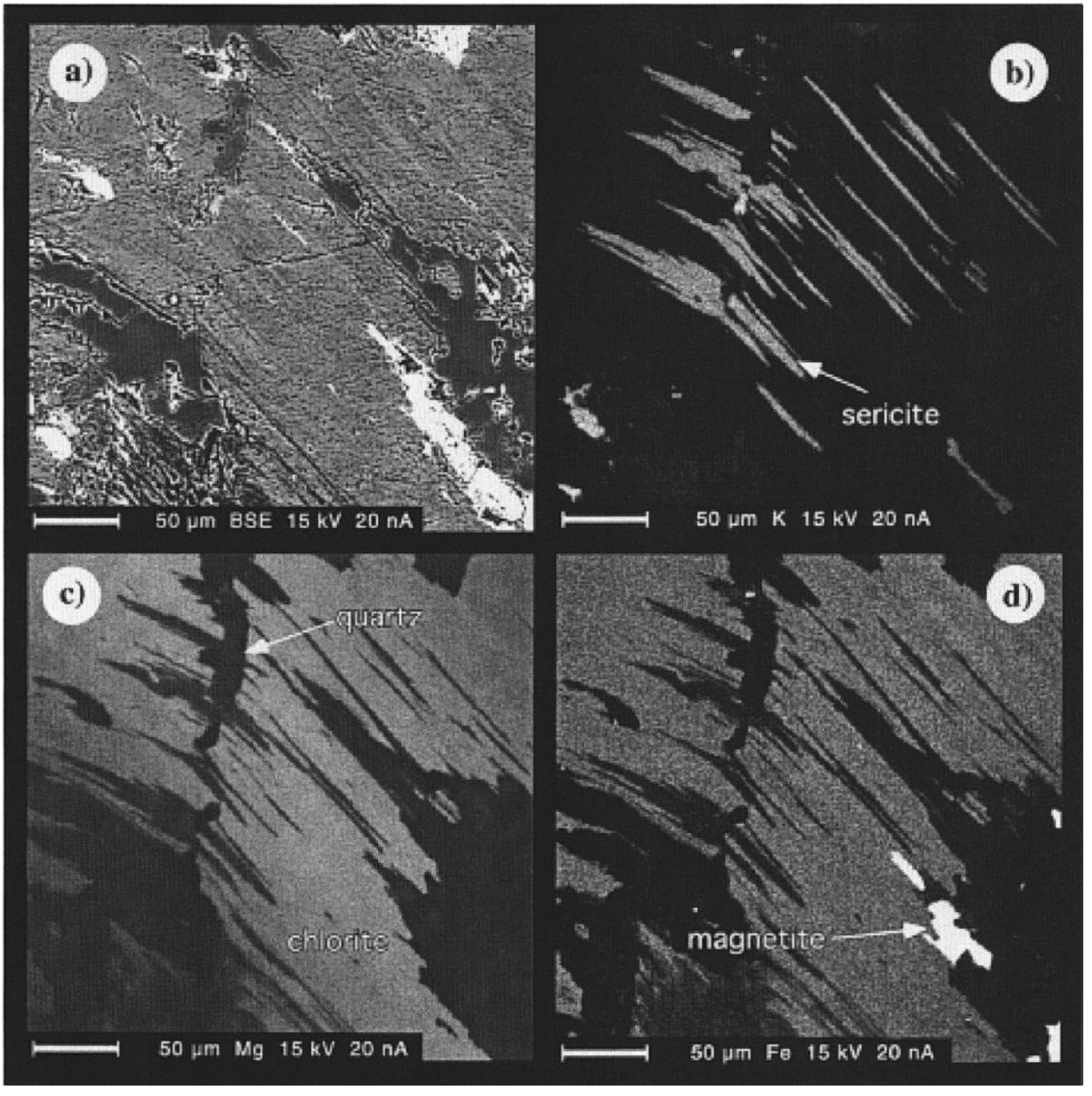

FIG. 4. Electron microprobe analysis of a chlorite-sericite-replaced biotite grain of stage 3 mineralized Osgood Mountains stock: (a) backscattered image; (b), (c), and (d) are X-ray elemental maps of K, Mg, and Fe, respectively. The sericite occurs as platelike intergrowths within the large chlorite grains which variably replace the Osgood Mountains stock biotite phenocrysts. The lack of Mg or Fe within the high K regions indicates that the high K phase is not remnant biotite within the chlorite grains.

chalcedonic quartz and calcite. Tectonic brecciation before, during, and after gold mineralization in stages 3 and 5 suggests that the Getchell fault was reactivated numerous times and was a conduit for hydrothermal fluids.

A detailed and complete study of mineral paragenesis for the Twin Creeks deposit was beyond the scope of this investigation and hindered by the lack of exposure of sulfide mineralization in the pits. Therefore an effort was made to determine if the five stages of mineralization identified at the Getchell deposit could also be supported by the limited sulfide material available from the Twin Creeks mine. Base metal mineralization ± gold, equivalent to stage 2 at the Getchell deposit, occurs along high-angle faults in close proximity to Cretaceous granodiorite dikes at the north end of the Twin Creeks mine. Ore mined at the Twin Creeks deposit is associated with argillic alteration and multiple episodes of hydrothermal silicification, equivalent to stage 3 at the Getchell deposit.

Decalcification and hydrothermal silicification are prominent alteration types associated with ores at the Twin Creeks mine, regardless of rock type or structural setting. Gold mineralization in the central and southern areas of the mine occurs as passive replacements along overturned fold limbs in the Valmy and Comus Formations. In contrast, ores at the

north end of the mine are characterized by zones of extreme decalcification and silicification near high-angle faults in the Etchart Formation. Realgar-quartz-pyrite-stibnite and orpiment-pyrite-gold mineralization, equivalent to stage 5 at the Getchell deposit, is located in vugs in highly silicified rocks of the Comus and Valmy Formations, or as veins that cut these rocks. The youngest gold mineralizing event recognized at the Twin Creeks mine is represented by stibnite veins which contain quartz, auriferous pyrite, and adularia. Carlin-type gold mineralization at the Getchell and Twin Creeks deposits would therefore consist of mineralization in stages 3 and 5. Although base metal mineralization in skarn is spatially associated with stages 3 and 5 of mineralization in the Main pit at the Getchell mine this does not imply a genetic association.

The regional distribution of the different stages of mineralization shows that skarn mineralization in stages 1 and 2 occurs as halos around Cretaceous intrusions, in contrast to stages 3 and 5 mineralization which occurs in a discrete area on the eastern flank of the Osgood Mountains. Stages 3 and 5 mineralization are not zoned relative to Cretaceous intrusions or mineralization in stages 1 and 2. Reactivation of regional structures, such as the Getchell fault zone, provided pathways for hydrothermal fluids over time and allowed the overprinting of multiple mineralizing events in restricted areas. Therefore skarn mineralization in stages 1 and 2 will not be considered to represent Carlin-type gold mineralization, which at the Getchell and Twin Creeks mines was produced by the overprinting of stage 3 by stage 5 mineralization.

Description of Samples for $^{40}Ar/^{39}Ar$ Dating

$^{40}Ar/^{39}Ar$ analyses were performed on 10 rock samples, which were specifically collected to assess the timing of gold mineralization relative to igneous activity and mineral paragenesis. Seven samples are from variably altered or mineralized igneous bodies at the Getchell property and three are vein adularia samples from the Twin Creeks and McCoy mines (Fig. 1c). Secondary minerals in igneous rocks include sericite after biotite and K feldspar after plagioclase. Sample location, geologic significance, and relationship to mineral paragenesis are detailed below. All samples except for 4 and 7 contain gold mineralization, as much as 10 ppm, although the siting of gold in the samples was never directly determined. Locations for all samples are shown in Figure 1b.

Samples

Sample 1, Getchell mine, North pit. Sampled material: pit exposure of fine-grained pyrite and hydrothermal quartz associated with stage 3 gold mineralization in a dacite dike. Mineralization is restricted to a fault that cuts the dike. Minerals separated: primary biotite phenocrysts, secondary K feldspar, and sericite with chlorite (Figs. 4, 5).

Sample 2, Getchell mine, Turquoise Ridge pit. Sampled material: pit exposure of dacite dike containing pyrrhotite (stage 1) that is overprinted by stage 3 quartz-pyrite-gold mineralization at depth. Minerals separated: primary biotite phenocrysts (3–5 mm).

Sample 3, Getchell property, 4 km northwest of Main pit. Sampled material: outcrop of stage 1 pyrrhotite-chalcopyrite-arsenopyrite-biotite mineralization in a highly sheared and silicified basalt. This Ordovician basalt flow underlies the Pennsylvanian to Permian limestone of the Etchart Formation. Minerals separated: hydrothermal biotite (2–4 mm).

Sample 4, Getchell property, 3 km east of Main pit. Sampled material: drill cuttings of an argillized granodiorite plug, spatially associated with stage 3 gold mineralization. Minerals separated: primary hornblende and secondary K feldspar (2–5 mm).

Sample 5, Getchell mine, Main pit. Sampled material: pit exposure of silicified, argillized, and stage 3 gold mineralized portion of the Osgood Mountains granodiorite stock in the footwall of the Getchell fault. Minerals separated: primary biotite phenocrysts, secondary K feldspar, and sericite within chlorite (Figs. 4, 5).

Sample 6, Getchell mine, underground. Sampled material: exposure in crosscut of a breccia pipe, containing clasts of pegmatitic quartz and K feldspar, which cuts high-grade quartz-pyrite-kaolinite-sericite mineralization. The breccia pipe contains stage 4 low-grade gold mineralization with pyrite in a siliceous matrix. The K feldspar clasts are inferred to be derived from a pegmatitic phase of the Osgood Mountains stock. Minerals separated: K feldspar, fragments of a single 3-cm crystal.

Sample 7, Getchell property, approximately 5 km southwest of the Getchell mine. Sampled material: outcrop of unaltered Osgood Mountains granodiorite stock, distal to any structural zones or known gold mineralization. Penecontemporaneous with stage 2 base metal ± gold and silver mineralization. Minerals separated: primary K feldspar (1–3 mm).

Sample 8, Twin Creeks mine, north of Twin Creeks fault zone. Sampled material: drill core of stage 5 high-grade massive stibnite vein with minor quartz, pyrite, and adularia, crosscuts barren basalt. Minerals separated: adularia, fine-grained (<1 mm). A clean separate of adularia from this sample was produced with difficulty due to large amounts of stibnite and pyrite contained in some of the adularia.

Sample 9, Twin Creeks mine, DZ fault zone. Sampled material: exposure in pit of silicified rocks with stage 5 quartz, pyrite, and adularia in vugs. Fluid inclusion microscopy of quartz from the DZ fault zone indicates that fluid boiling occurred during gold mineralization, and gold is commonly recognized as coarse disseminations (Groff, 1996). Minerals separated: adularia, coarse-grained (2 mm) crystals, some contain pyrite.

Sample 10, McCoy mine. Sampled material: exposure in pit of endoskarn containing quartz-pyrite-gold- adularia mineralization. Minerals separated: adularia, coarse (2 mm) crystals. The distribution of all the mineralization stages is shown in Figure 6 and the sample locations in Figure 1c.

Sample Preparation and Analytical Methods

Mineral separates were obtained by standard magnetic, heavy liquid, and handpicking techniques. Hand specimens from the Getchell property were crushed to 2 to 3 mm and hornblende and biotite were separated using a binocular microscope. K feldspar samples were obtained by heavy liquid floatation and sericite was concentrated by handpicking chlorite-replaced biotite phenocrysts. Adularia was handpicked from pit and drill core samples from the Twin Creeks and McCoy mines. All mineral separates were ultrasonically cleaned in dilute hydrochloric acid and distilled water to remove calcite.

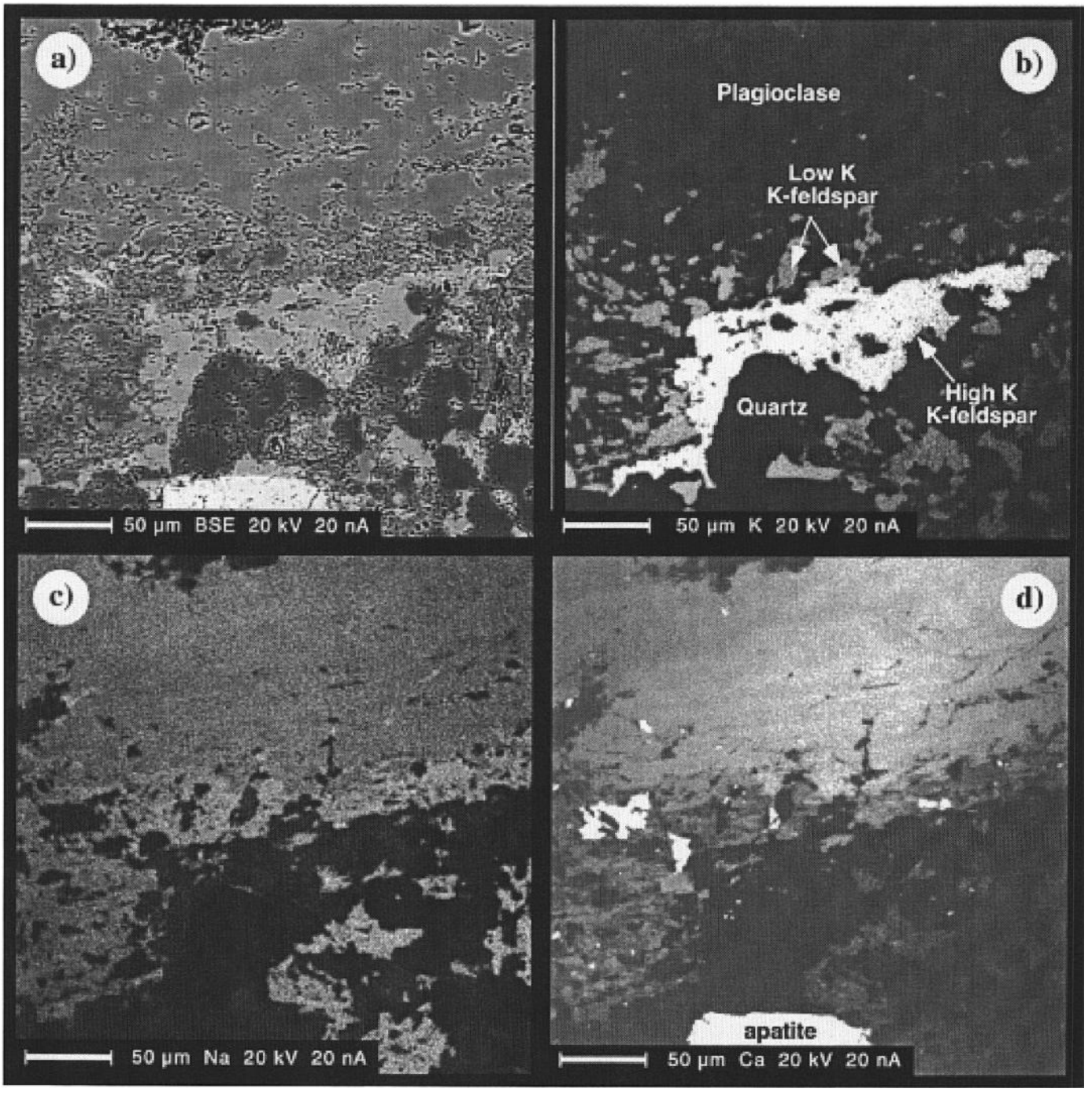

FIG. 5. Electron microprobe analysis of a secondary K feldspar rimming plagioclase within stage 3 mineralized Osgood Mountains stock: (a) backscattered image; (b), (c), and (d) X-ray elemental maps of K, Na, and Ca, respectively. Two distinct K feldspar populations are prominently shown by the K map and may reflect discrete mineral growth at ca. 83 and 75 Ma.

Samples were loaded in Sn, Al, or Cu foil packets, and in some cases in aluminum trays, and irradiated in evacuated quartz or Pyrex tubes in several packages in the Ford reactor at the University of Michigan and the Texas A and M reactor (Tables 1, 2). Fish Canyon tuff sanidine (27.84 Ma relative to 520.4 Ma for sample Mmhb-1; Samson and Alexander, 1987) was used as a flux monitor.

All samples from the Getchell, Twin Creeks, and McCoy mines were step heated in a double-vacuum tantalum or molybdenum resistance furnace, and argon measurements were made on a MAP 215-50 mass spectrometer operated in electron multiplier mode with a net sensitivity of 2 to 3×10^{-17} moles/pA. Uncertainties in ages are quoted at 2σ and include the ± 0.5 percent 2σ error in the calculated J factor. Total gas ages are calculated using the percent ^{39}Ar associated with each step as a weighting factor. Plateau ages are calculated

TABLE 1. Argon Isotope Data for Hornblende, Biotite, and Sericite

Temperature (°C)	$^{40}Ar/^{39}Ar^{1}$	$^{37}Ar/^{39}Ar^{1,2,3}$	$^{36}Ar/^{39}Ar^{1}$ (1×10^{-3})	$^{39}Ar_K$ moles	$^{40}Ar^{*1}$ (%)	% $^{39}Ar_K$ (released)	Age (Ma)	Error (Ma 2σ)
Sample 1: biotite, L#3170, J = 0.001610; 1.0 mg (NM-30)								
850	52.43	—	59.42	2.0×10^{-16}	66.6	3.61	98.7	2.9
900	38.50	—	10.57	3.3×10^{-16}	91.9	9.57	100.0	1.4
940	35.90	—	4.170	3.9×10^{16}	96.5	16.7	97.9	1.1
1,000	35.17	—	4.521	1.1×10^{-16}	96.3	18.8	95.8	3.7
1,040	37.09	—	9.190	3.9×10^{-16}	92.8	25.8	97.3	1.3
1,100	36.55	—	3.927	3.8×10^{-16}	96.8	32.6	100.0	1.2
1,200	35.38	—	2.102	9.8×10^{-16}	99.0	50.5	99.16	0.69
1,300	35.08	—	1.601	2.5×10^{-15}	98.7	96.1	97.84	0.53
1,600	33.99	—	4.875	2.1×10^{-16}	95.8	100	92.2	6.3
Total gas age n = 9				5.5×10^{-15}			98.1	1.1
Sample 1: sericite, L#1203, J = 0.000677; 4.0 mg (NM-13)								
650	159.2	0.0560	311.8	1.4×10^{-15}	42.1	8.40	80.2	2.8
800	86.57	0.0713	56.30	2.8×10^{-15}	80.8	25.4	83.5	1.2
850	78.00	0.0072	26.40	2.1×10^{-15}	90.0	38.1	83.8	1.0
900	77.11	0.0048	25.20	2.9×10^{-15}	90.3	55.7	83.18	0.59
1,000	77.07	0.0051	23.80	3.6×10^{-15}	90.9	78.1	83.61	0.91
1,100	75.20	0.0158	18.70	2.0×10^{-15}	92.6	90.4	83.16	0.74
1,200	73.98	0.0755	27.80	1.0×10^{-15}	88.9	96.9	78.62	0.85
1,650	64.38	0.8610	36.70	5.0×10^{-16}	83.2	100	64.34	0.94
Total gas age N = 8				1.6×10^{-14}			82.3	1.1
Sample 2: biotite, L#2098, J = 0.000739; 1.4 mg (NM-20)								
600	320.3	0.0254	905.2	2.2×10^{-16}	16.5	1.17	69.0	6.3
670	122.0	0.0285	151.9	2.5×10^{-16}	63.2	2.48	99.9	2.2
740	89.72	0.0061	44.00	9.3×10^{-16}	85.5	7.38	99.42	0.79
800	79.26	0.0041	12.90	2.0×10^{-15}	95.2	18.0	97.84	0.42
840	77.90	0.0081	8.630	1.3×10^{-15}	96.7	24.9	97.71	0.47
870	78.24	0.0171	12.50	5.7×10^{-16}	95.2	27.9	96.67	0.76
900	77.37	0.0450	11.70	3.2×10^{-16}	95.5	29.6	95.9	1.2
940	79.65	0.0328	26.20	2.7×10^{-16}	90.2	31.0	93.4	1.3
1,000	78.49	0.0201	23.89	4.0×10^{-16}	91.0	33.1	92.8	1.1
1,040	78.33	0.0198	20.44	4.7×10^{-16}	92.3	35.6	93.8	1.0
1,100	77.62	0.0084	13.80	1.3×10^{-15}	94.7	42.4	95.42	0.56
1,150	76.71	0.0063	11.00	3.0×10^{-15}	95.7	58.0	95.31	0.37
1,200	75.46	0.0026	6.980	4.2×10^{-15}	97.2	79.9	95.24	0.33
1,650	75.45	0.0119	14.10	3.8×10^{-15}	94.4	100	92.56	0.40
Total gas age n = 14				1.9×10^{-14}			95.07	0.75
Sample 3: biotite, L#1204, J = 0.0006800; 1.2 mg (NM-13)								
670	564.9	0.0587	1,696	2.2×10^{-16}	11.3	2.40	76	12
800	90.28	0.0094	37.60	1.8×10^{-15}	87.7	22.8	94.5	0.69
850	82.97	0.0040	4.420	1.9×10^{-15}	98.4	44.3	97.4	0.73
1,000	84.54	0.0071	5.190	1.7×10^{-15}	98.2	62.8	99.0	0.73
1,100	81.44	0.0086	2.010	1.4×10^{-15}	99.2	78.6	96.5	0.59
1,650	78.45	0.0193	1.950	1.9×10^{-15}	99.2	100	93.0	0.88
Total gas age n = 6				9.0×10^{-15}			95.5	1.1
Sample 4: hornblende, L#5565, J = 0.001437; 16.0 mg (NM-38)								
700	2,601	8.686	8,518	8.0×10^{-17}	3.30	0.871	208	210
800	415.7	3.271	1,210	3.6×10^{-17}	14.1	1.26	146	48
900	513.5	3.372	1,566	6.0×10^{-17}	9.90	1.92	128	47
1,000	99.51	6.469	207.0	2.1×10^{-16}	39.0	4.18	98.4	4.1
1,040	60.68	8.177	73.40	3.1×10^{-16}	65.3	7.58	100.4	2.2
1,070	49.41	8.098	34.60	2.1×10^{-16}	80.6	9.87	100.9	2.3
1,100	45.52	8.212	25.30	5.6×10^{-16}	85.0	16.0	98.1	1.4
1,150	44.61	8.083	24.70	3.0×10^{-15}	85.0	48.4	96.26	0.63
1,200	39.65	8.010	9.730	4.2×10^{-15}	94.3	94.2	94.92	0.49
1,250	48.18	9.527	37.30	3.6×10^{-16}	78.6	98.1	96.2	1.5
1,400	73.07	11.36	116.6	1.8×10^{-16}	54.1	100	100.4	4.1
Total gas age n = 11				9.2×10^{-15}			97.5	3.2

TABLE 1. (*Cont.*)

Temperature (°C)	$^{40}Ar/^{39}Ar^{1}$	$^{37}Ar/^{39}Ar^{1,2,3}$	$^{36}Ar/^{39}Ar^{1}$ (1×10^{-3})	$^{39}Ar_K$ moles	$^{40}Ar°^{1}$ (%)	% $^{39}Ar_K$ (released)	Age (Ma)	Error (Ma 2σ)
Sample 5: biotite, L#64, J = 0.004260; 1.0 mg (NMUM-1)								
650	17.01	—	26.90	4.1×10^{-16}	53.2	0.606	68.2	2.9
730	76.42	—	216.6	1.8×10^{-15}	16.2	3.29	92.9	7.0
800	14.17	—	6.66	7.4×10^{-15}	86.0	14.2	91.26	0.56
900	12.97	—	2.14	8.0×10^{-15}	95.0	26.1	92.31	0.58
1,000	13.23	—	2.48	5.6×10^{-15}	94.3	34.4	93.47	0.53
1,100	12.75	—	1.28	1.7×10^{-14}	96.9	60.1	92.56	0.47
1,200	12.38	—	0.34	1.9×10^{-14}	99.0	88.7	91.85	0.43
1,300	13.41	—	3.87	3.6×10^{-15}	91.3	93.9	91.73	0.61
1,600	11.65	—	2.72	4.1×10^{-15}	92.9	100	81.35	0.77
Total gas age n = 9				6.7×10^{-14}			91.40	0.84
Sample 5: sericite, L#65, J = 0.004260; 1.3 mg (NMUM-1)								
600	12.20	—	3.910	9.6×10^{-16}	90.4	5.75	82.8	1.3
700	48.95	—	126.4	2.9×10^{-15}	23.7	23.4	87.0	4.1
800	13.53	—	8.210	4.9×10^{-15}	81.9	53.0	83.27	0.65
900	12.82	—	7.500	3.6×10^{-15}	82.6	74.4	79.55	0.62
1,000	14.36	—	13.70	2.0×10^{-15}	71.8	86.6	77.51	0.88
1,100	14.95	—	16.70	1.1×10^{-15}	66.9	93.1	75.2	1.5
1,250	12.47	—	8.470	9.1×10^{-16}	79.8	98.6	74.9	1.2
1,600	13.98	—	10.30	2.3×10^{-16}	78.0	100	81.9	3.6
Total gas age n = 8				1.7×10^{-14}			81.4	1.4

L# = lab identification number, NM and NMUM = irradiation package identification.
[1] Blank corrected
[2] Corrected for ^{37}Ar decay
[3] Dash indicates no detectable ^{37}Ar due to long hiatus between irradiation and analysis

using the inverse of the variance as the weighting factor for the steps that define the plateau. Isochron regressions were performed by the method described by York (1969). All age data, including published results, are calculated using the decay constants and isotopic abundances recommended by Steiger and Jager (1977). The argon closure temperatures for hornblende and biotite are assumed to be 500° and 300°C, respectively (Harrison, 1981; Harrison et al., 1985). Further details of argon extraction are given in McIntosh and Cather (1994).

Backscattered electron images and X-ray elemental maps were produced using a CAMECA SX-100 microprobe equipped with three wavelength dispersive spectrometers and high-speed backscattered electron detectors. The microprobe beam was held at 15 kV and 20 nA for the acquisition of both the X-ray maps and backscattered images.

$^{40}Ar/^{39}Ar$ Results

A total of 15 mineral separates of hornblende, biotite, sericite, K feldspar, and vein adularia from the Getchell, Twin Creeks, and McCoy mines were dated using the $^{40}Ar/^{39}Ar$ step-heating technique (Tables 1, 2). Some of the samples yielded complex age spectra, presumably due to varying degrees of alteration, incomplete replacement of primary phases by secondary minerals, nonatmospheric trapped argon components, and/or recoil of ^{39}Ar during irradiation. We note that none of the dated samples are sufficiently fine grained (<0.1 μm) to have ^{39}Ar recoil loss be a problem, but internal features, such as chlorite alteration of biotite, could cause ^{39}Ar redistribution within the minerals, thus producing complex age spectra. The complexity of the argon results leads to instances where precise age determinations are not always possible and where more than one data-handling method could be used to determine an apparent age. First, we chose the plateau age when one was obtained. Second, if age spectrum discordance can be rationalized through statistically meaningful isochron analysis, the isochron age is quoted. Finally, if excessive scatter occurs in both the age spectrum and isochron, the total gas age is given as the best apparent age estimate.

Sample 1 primary biotite yields a somewhat undulatory age spectrum with a total gas age of 98.1 ± 1.2 Ma (Fig. 7a). An isochron with a mean square weighted deviation (MSWD) of 5.2, which uses all of the heating steps, yields an age of 98.4 ± 0.6 Ma and an $^{40}Ar/^{36}Ar_i$ of 302 ± 16 (Fig. 8a). Despite the relatively high MSWD, the isochron age is interpreted to be the best estimate for the apparent age of this biotite.

Sample 2 primary biotite yields an undulatory age spectrum (Fig. 7b). Isochron analysis does not yield a simple linear data array; therefore, the age spectrum discordance may be explained by a complex mixture of nonatmospheric argon and/or ^{39}Ar recoil associated with alteration phases (Lo and Onstott, 1989). Due to the complexity of the age spectrum and isochron, we interpret the total gas age of 95.1 ± 0.7 Ma to represent the apparent age of this biotite.

The age spectrum for sample 3 hydrothermal biotite (Fig. 7b) is older in the intermediate steps than in the initial and late heating steps. This hump-shaped age spectrum form is common for biotite, and in cases where the rock age can be constrained by other methods, it has been shown that the total gas age of these hump-shaped biotites yields geologically consistent results (Hubacher and Lux, 1987; Heizler et al.,

TABLE 2. Argon Isotope Data for K Feldspars, plus Kinetic Data

Temperature (°C)	$^{40}Ar/^{39}Ar$[1]	$^{37}Ar/^{39}Ar$[1,2,3]	$^{36}Ar/^{39}Ar$[1] (1×10^{-3})	$^{39}Ar_K$ moles	$\%^{39}Ar^{\circ}$[1]	$\%^{39}Ar_K$ (released)	Age (Ma)	Error (Ma ± 2σ)	Heating time (min)	log (D/r^2) (/sec)
Sample 5: K-feldspar, L#66, J = 0.004260; 1.1 mg (NMUM-1)										
500	8.26	—	6.870	1.9×10^{-16}	75.2	0.744	47.1	3.1	6	−6.92
600	9.12	—	3.570	5.1×10^{-16}	88.2	2.77	60.8	1.2	6	−5.82
650	16.02	—	23.80	8.7×10^{-16}	56.0	6.23	67.7	1.3	6	−5.17
700	151.8	—	479.2	6.1×10^{-16}	6.70	8.65	77	16	6	−5.11
750	30.06	—	64.10	1.2×10^{-15}	36.9	13.6	83.4	2.4	6	−4.63
800	14.21	—	11.00	1.2×10^{-15}	77.0	18.5	82.22	0.84	6	−4.47
850	16.50	—	18.90	1.5×10^{-15}	66.0	24.4	81.80	0.94	6	−4.27
900	11.41	—	1.970	3.2×10^{-15}	94.7	37.0	81.21	0.49	6	−3.78
950	11.20	—	1.900	2.3×10^{-15}	94.8	46.4	79.83	0.46	6	−3.78
1,000	11.33	—	2.360	2.7×10^{-14}	93.7	57.0	79.80	0.49	6	−3.62
1,050	11.20	—	2.380	3.6×10^{-15}	93.6	71.3	78.81	0.46	6	−3.35
1,100	11.13	—	2.600	2.3×10^{-15}	92.9	80.3	77.78	0.49	6	−3.39
1,150	10.80	—	1.860	2.8×10^{-15}	94.8	91.5	76.97	0.46		
1,200	10.90	—	2.070	1.5×10^{-15}	94.2	97.3	77.27	0.59		
1,700	10.79	—	2.060	6.8×10^{-16}	94.2	100	76.45	0.82		
Total gas age n = 15				4.91×10^{-14}			78.4	1.1		
Sample 1: K feldspar, L#2101, J = 0.000675; ~1 mg (NM-13)										
500	1446	—	4,635	2.8×10^{-16}	5.30	0.687	91	26	10	−7.21
500	352.4	—	986.1	9.2×10^{-17}	17.3	0.913	73	12	20	−7.63
550	414.1	—	1,220	1.9×10^{-16}	13.0	1.38	64.4	7.7	10	−6.85
550	188.7	—	442.2	1.9×10^{-16}	30.8	1.86	69.3	4.6	20	−7.00
600	373.1	—	1,077	3.7×10^{-16}	14.7	2.75	65.8	6.3	10	−6.27
600	147.9	—	295.6	3.5×10^{-16}	41.0	3.62	72.4	2.4	20	−6.44
650	217.2	—	537.2	4.9×10^{-16}	26.9	4.82	69.9	2.9	10	−5.88
650	115.2	—	117.2	4.7×10^{-16}	54.6	5.96	75.1	1.8	20	−6.10
700	129.2	—	224.7	4.4×10^{-16}	48.7	7.04	75.0	1.9	10	−5.74
700	89.62	—	84.90	5.1×10^{-16}	72.1	8.27	77.0	1.1	20	−5.91
750	100.7	—	122.9	5.2×10^{-16}	64.0	9.54	76.8	1.3	10	−5.53
750	85.30	—	69.70	5.4×10^{-16}	75.9	10.9	77.2	1.0	20	−5.75
800	100.2	—	113.7	5.7×10^{-16}	66.5	12.3	79.4	1.1	10	−5.37
800	82.01	—	53.50	5.8×10^{-16}	80.8	13.7	78.95	0.85	20	−5.62
850	92.13	—	90.80	5.3×10^{-16}	70.9	15.0	77.9	1.0	10	−5.31
900	110.0	—	152.1	1.1×10^{-15}	59.2	17.6	77.55	0.87	10	−4.95
1,000	96.61	—	101.5	5.8×10^{-15}	69.0	31.8	79.32	0.55	10	−4.04
1,100	81.00	—	53.00	6.2×10^{-15}	80.7	47.0	77.83	0.40	10	−3.80
1,150	88.40	—	81.40	3.6×10^{-15}	72.8	55.7	76.70	0.46		
1,200	97.34	—	114.1	2.8×10^{-15}	65.4	62.6	75.88	0.64		
1,300	95.95	—	104.9	6.6×10^{-15}	67.8	78.7	77.47	0.51		
1,400	77.35	—	33.80	8.1×10^{-15}	87.1	98.4	80.24	0.36		
1,500	98.32	—	73.20	6.5×10^{-16}	78.9	100	92.7	1.0		
Total gas age n = 23				4.09×10^{-14}			78.1	1.0		
Sample 7: K feldspar, L#2443, J = 0.000673; ~1 mg (NM-13)										
450	678.2	—	2,083	2.9×10^{-17}	10.0	0.440	85	52	10	−7.57
450	386.7	—	1,118	1.1×10^{-17}	16.1	0.607	78	56	20	−7.91
500	382.3	—	1,167	1.5×10^{-17}	9.80	0.826	45	60	10	−7.38
500	159.1	—	404.9	1.9×10^{-17}	24.8	1.11	47	22	20	−7.43
550	227.4	—	591.7	3.0×10^{-17}	23.1	1.57	63	18	10	−6.79
550	96.43	—	156.1	3.4×10^{-17}	52.1	2.08	60.0	8.6	20	−6.91
600	188.9	—	441.8	4.7×10^{-17}	30.9	2.79	69	11	10	−6.35
600	81.12	—	84.80	5.7×10^{-17}	69.1	3.66	66.8	4.8	20	−6.44
650	174.4	—	381.7	6.1×10^{-17}	35.4	4.57	73.6	8.3	10	−6.01
900	97.02	—	73.20	5.4×10^{-16}	78.7	35.6	91.2	1.0	20	−4.47
950	105.9	—	106.0	7.3×10^{-16}	71.1	46.5	89.8	1.0	20	−4.23
1,000	93.79	—	61.20	6.9×10^{-16}	81.4	56.9	90.92	0.86	20	−4.15
1,050	87.06	—	42.30	4.7×10^{-16}	86.6	63.9	89.9	1.0	20	−4.22
1,100	81.23	—	21.10	2.9×10^{-16}	93.3	68.3	90.4	1.2	20	−4.36
1,100	81.97	—	33.60	1.5×10^{-16}	89.5	70.6	88.0	2.0	30	−4.77
1,100	91.04	—	60.90	1.3×10^{-16}	81.1	72.6	88.2	2.5	60	−5.10
1,100	97.61	—	68.10	7.0×10^{-17}	79.7	73.6	92.3	4.2	120	−5.66
1,200	99.07	—	80.70	1.5×10^{-16}	77.6	75.9	92.4	2.4	20	
1,250	108.8	—	102.3	1.2×10^{-16}	67.9	77.6	88.0	2.8	10	
1,300	102.8	—	88.10	3.8×10^{-16}	75.0	83.3	91.5	1.2	10	
1,350	147.8	—	222.5	1.9×10^{-16}	55.9	86.1	98.2	2.7	10	
1,400	180.8	—	318.8	2.0×10^{-16}	48.3	89.1	103.7	3.2	10	
1,500	133.4	—	171.4	6.6×10^{-16}	62.8	99.1	99.9	1.5	10	
1,800	462.0	—	1,491	6.2×10^{-17}	5.60	100	33	61	10	
Total gas age n = 32				6.7×10^{-15}			88.9	2.9		

TABLE 2. (*Cont.*)

Temperature (°C)	$^{40}Ar/^{39}Ar$[1]	$^{37}Ar/^{39}Ar$[1,2,3]	$^{36}Ar/^{39}Ar$[1] (1×10^{-3})	$^{39}Ar_K$ moles	$\%^{39}Ar$[a1]	$\%^{39}Ar_K$ (released)	Age (Ma)	Error (Ma $\pm 2\sigma$)	Heating time (min)	log (D/r^2) (/sec)
Sample 6: K feldspar, L#2449, J = 0.002271; 14.9 mg (NM-23)										
450	554.5	0.0242	1,363	1.0×10^{-15}	27.4	0.142	534	18	10	−8.59
450	82.03	0.0000	181.6	2.6×10^{-16}	34.6	0.178	112.5	8.4	20	−9.13
500	88.15	0.0147	152.1	4.0×10^{-16}	49.0	0.233	168.8	4.9	10	−8.53
500	36.76	0.0072	58.71	5.5×10^{-16}	52.7	0.310	77.7	3.5	20	−8.57
550	47.72	0.0082	66.1	1.0×10^{-15}	59.0	0.450	111.8	2.1	10	−7.86
550	22.44	0.0079	14.4	1.3×10^{-15}	81.0	0.628	73.0	1.2	20	−7.91
600	29.88	0.0092	24.6	2.3×10^{-15}	75.6	0.947	90.2	1.1	10	−7.19
600	19.68	0.0085	4.160	2.7×10^{-15}	93.6	1.32	73.96	0.63	20	−7.26
650	24.71	0.0148	13.5	3.3×10^{-15}	83.8	1.79	82.86	0.61	10	−6.73
650	19.64	0.0132	3.610	4.9×10^{-15}	94.5	2.46	74.45	0.41	20	−6.73
700	21.84	0.0127	7.420	6.4×10^{-15}	89.9	3.35	78.68	0.42	10	−6.18
700	19.29	0.0103	1.450	7.4×10^{-15}	97.7	4.38	75.59	0.38	20	−6.29
750	20.28	0.0078	2.390	8.3×10^{-15}	96.4	5.53	78.40	0.39	10	−5.83
750	19.83	0.0056	0.8050	1.1×10^{-14}	98.7	7.04	78.47	0.35	20	−5.91
800	20.42	0.0049	1.380	1.1×10^{-14}	97.9	8.63	80.09	0.41	10	−5.49
800	20.30	0.0043	0.3920	1.5×10^{-14}	99.3	10.7	80.76	0.37	20	−5.59
850	20.94	0.0032	0.7200	2.7×10^{-14}	98.9	14.5	82.90	0.35	20	−5.21
900	21.38	0.0022	0.5210	3.5×10^{-14}	99.2	19.4	84.83	0.35	20	−4.97
950	21.76	0.0022	0.2410	4.3×10^{-14}	99.6	25.3	86.66	0.32	20	−4.77
1,000	22.05	0.0041	0.2710	4.5×10^{-14}	99.5	31.5	87.76	0.33	20	−4.64
1,050	22.38	0.0069	0.3390	4.2×10^{-14}	99.5	37.3	88.96	0.33	20	−4.59
1,100	22.80	0.0165	0.3250	3.7×10^{-14}	99.5	42.5	90.62	0.35	20	−4.57
1,100	23.09	0.0072	0.3650	2.5×10^{-14}	99.4	45.9	91.69	0.37	30	−4.88
1,100	23.25	0.0038	0.5910	2.4×10^{-14}	99.2	49.3	92.08	0.39	60	−5.16
1,100	23.40	0.0028	0.8800	2.4×10^{-14}	98.8	52.7	92.31	0.42	120	−5.44
1,100	23.45	0.0029	1.600	3.4×10^{-14}	97.9	57.3	91.69	0.36	323	−5.67
1,100	24.01	0.0034	3.103	3.5×10^{-14}	96.1	62.2	92.11	0.39	1,078	−6.13
1,300	23.50	0.0073	1.260	2.5×10^{-14}	98.3	65.6	92.28	0.39		
1,400	23.36	0.0016	1.940	2.1×10^{-13}	97.5	95.2	90.95	0.41		
1,750	24.57	0.0048	4.790	3.4×10^{-14}	94.2	100	92.37	0.39		
Total gas age n = 30				7.2×10^{-13}			89.54	0.61		
Sample 4: K feldspar, L#5562, J = 0.001438; 13.4 mg (NM-38)										
400	10,540	0.5046	35,345	3.2×10^{-17}	0.90	0.065	233	309	10	−9.26
400	3,009	0.4815	10,052	4.5×10^{-17}	1.30	0.154	99	431	20	−8.89
475	679.2	0.4124	2,199	1.2×10^{-16}	4.30	0.401	75	46	10	−7.75
475	439.9	0.3858	1,400	1.9×10^{-16}	6.00	0.780	67	25	20	−7.53
550	280.4	0.3543	827.3	4.9×10^{-16}	12.8	1.76	91	10	10	−6.48
550	134.9	0.3613	357.3	5.1×10^{-16}	21.7	2.80	74.6	5.0	20	−6.51
600	113.4	0.3725	277.5	9.1×10^{-16}	27.7	4.63	79.8	3.5	10	−5.75
600	71.10	0.3911	134.7	8.6×10^{-16}	44.1	6.36	79.5	2.1	20	−5.90
650	96.65	0.4358	214.3	1.4×10^{-15}	34.5	9.09	84.6	2.5	10	−5.26
650	61.79	0.5280	95.80	1.1×10^{-15}	54.2	11.4	85.0	1.6	20	−5.51
700	72.57	0.6455	130.6	1.2×10^{-15}	46.9	13.8	86.3	1.8	10	−5.10
700	54.01	0.5741	67.70	1.1×10^{-15}	63.0	16.1	86.3	1.2	20	−5.34
750	64.23	0.7675	101.7	1.0×10^{-15}	53.3	18.2	86.8	1.7	10	−5.03
750	49.37	0.4016	50.60	1.0×10^{-15}	69.8	20.3	87.2	1.1	20	−5.28
800	55.36	0.5654	72.00	8.5×10^{-16}	61.7	22.0	86.5	1.6	10	−5.02
800	51.14	0.4508	58.00	9.2×10^{-16}	66.5	23.9	86.2	1.2	20	−5.25
850	58.01	0.6517	82.50	1.3×10^{-15}	58.0	26.5	85.4	1.3	20	−5.07
900	64.96	0.7138	106.2	1.5×10^{-15}	51.8	29.5	85.2	1.5	20	−4.96
950	64.68	0.6132	106.7	2.1×10^{-15}	51.3	33.7	84.2	1.4	20	−4.76
1,000	55.15	0.7044	73.60	2.6×10^{-15}	60.6	39.0	84.8	1.0	20	−4.60
1,050	52.00	0.4846	65.70	2.7×10^{-15}	62.7	44.5	82.7	1.0	20	−4.52
1,100	55.71	0.2992	77.20	3.3×10^{-15}	59.1	51.1	83.5	1.1	20	−4.39
1,100	55.94	0.2928	78.90	2.3×10^{-15}	58.3	55.8	82.8	1.1	30	−4.64
1,100	56.60	0.3269	80.20	2.3×10^{-15}	58.2	60.3	83.5	1.2	60	−4.91
1,100	58.43	0.3701	86.40	2.2×10^{-15}	56.4	64.9	83.5	1.2	120	−5.17
1,100	63.13	0.4052	101.2	2.2×10^{-15}	52.7	69.4	84.3	1.4	240	−5.41
1,100	69.15	0.4319	119.1	8.4×10^{-16}	49.1	71.1	86.1	1.9	155	−5.61
1,250	102.2	0.5269	232.7	5.1×10^{-15}	32.8	81.4	84.8	2.6		
1,300	102.3	0.4658	229.0	6.4×10^{-15}	33.9	94.2	87.9	2.4		
1,400	294.9	3.079	853.4	2.2×10^{-15}	14.6	98.7	108.4	8.6		
1,750	294.0	8.405	809.1	6.2×10^{-16}	18.9	100	139.6	9.1		
Total gas age n = 31				5.0×10^{-14}			86.5	4.8		

TABLE 2. (*Cont.*)

Temperature (°C)	$^{40}Ar/^{39}Ar$[1]	$^{37}Ar/^{39}Ar$[1,2,3]	$^{36}Ar/^{39}Ar$[1] (1×10^{-3})	$^{39}Ar_K$ moles	$\%^{39}Ar^{\circ}$[1]	$\%^{39}Ar_K$ (released)	Age (Ma)	Error (Ma ± 2σ)	Heating time (min)	log (D/r^2) (/sec)
Sample 8: adularia, L#1202, J = 0.0006712; ~1 mg (NM-13)										
750	171.8	0.0045	458.4	9.6×10^{-16}	21.1	2.74	43.4	2.8	10	−6.01
850	44.80	0.0008	31.84	2.3×10^{-15}	79.0	9.43	42.33	0.39	10	−5.23
950	36.18	0.0000	3.140	4.4×10^{-15}	97.4	21.9	42.16	0.33	10	−4.69
1,050	35.07	0.0022	0.0119	5.4×10^{-15}	99.9	37.3	41.94	0.26	10	−4.51
1,150	34.97	0.0004	—	6.1×10^{-15}	100	54.6	41.90	0.36	10	−4.41
1,200	35.19	0.0000	—	4.3×10^{-15}	100	66.8	42.11	0.34		
1,300	35.13	0.0000	0.2480	5.0×10^{-15}	99.7	81.2	41.93	0.26		
1,450	35.36	0.0005	—	6.4×10^{-15}	100	99.5	42.31	0.28		
1,650	37.69	0.1984	15.80	1.7×10^{-16}	87.6	100	39.5	1.3		
Total gas age n = 9				3.5×10^{-14}			42.10	0.42		
Sample 9: adularia, L#2099, J = 0.0007368; ~5 mg (NM-20)										
600	294.9	0.0152	899.4	2.8×10^{-16}	9.90	0.213	38.3	4.9	10	−8.23
750	37.39	—	13.50	1.3×10^{-15}	89.3	1.22	43.83	0.34	10	−6.73
850	33.96	—	5.610	3.9×10^{-15}	95.1	4.27	42.41	0.18	10	−5.66
900	32.57	—	1.840	4.4×10^{-15}	98.3	7.68	42.05	0.17	10	−5.27
950	32.22	—	0.8250	5.9×10^{-15}	99.2	12.2	41.98	0.15	10	−4.92
1,000	32.07	—	0.5090	7.4×10^{-15}	99.5	17.9	41.91	0.15	10	−4.65
1,050	32.09	0.0002	0.7820	8.8×10^{-15}	99.2	24.7	41.84	0.15	10	−4.42
1,100	32.02	0.0003	0.7460	1.1×10^{-14}	99.3	32.9	41.75	0.14	10	−4.21
1,150	32.04	0.0001	0.7100	1.2×10^{-14}	99.3	42.1	41.79	0.13		
1,200	32.36	0.0001	1.280	1.0×10^{-14}	98.8	50.0	42.00	0.17		
1,250	32.20	—	1.050	9.8×10^{-15}	99.0	57.5	41.88	0.15		
1,300	32.30	0.0002	1.250	9.2×10^{-15}	98.8	64.7	41.92	0.13		
1,350	32.40	0.0002	1.420	1.5×10^{-14}	98.6	76.4	41.99	0.12		
1,400	32.14	—	0.7560	2.5×10^{-14}	99.2	95.9	41.91	0.12		
1,500	32.98	—	2.530	5.1×10^{-15}	97.7	99.9	42.31	0.14		
1,750	445.8	0.0040	1,383	1.8×10^{-16}	8.30	100	49	11		
Total gas age n = 16				1.3×10^{-13}			41.96	0.27		
Sample 10: adularia, L#2100, J = 0.0007375; ~5 mg (NM-20)										
600	798.0	0.0468	2,558	3.5×10^{-16}	5.30	0.389	55	14	10	−7.64
750	63.73	0.0066	108.2	1.5×10^{-15}	49.8	2.07	41.74	0.63	10	−6.20
850	32.02	0.0028	8.710	2.9×10^{-15}	91.9	5.27	38.74	0.21	10	−5.45
900	29.46	0.0023	1.410	2.5×10^{-15}	98.5	8.02	38.21	0.21	10	−5.26
950	29.01	0.0012	−0.298	2.8×10^{-15}	100	11.2	38.29	0.18	10	−5.04
1,000	30.71	0.0005	5.220	3.2×10^{-15}	94.9	14.7	38.37	0.16	10	−4.86
1,050	29.49	0.0019	1.240	3.9×10^{-15}	98.7	19.1	38.31	0.15	10	−4.65
1,100	29.58	0.0031	1.480	4.3×10^{-15}	98.5	23.9	38.34	0.13	10	−4.51
1,150	30.66	0.0076	5.720	4.2×10^{-15}	94.4	28.6	38.12	0.15		
1,200	31.47	0.0068	8.510	3.3×10^{-15}	91.9	32.3	38.09	0.18		
1,250	30.98	0.0084	6.770	3.9×10^{-15}	93.5	36.6	38.13	0.16		
1,300	30.49	0.0093	5.070	8.9×10^{-15}	95.0	46.6	38.15	0.14		
1,350	30.02	0.0050	3.310	1.6×10^{-14}	96.7	64.6	38.20	0.11		
1,400	30.44	0.0038	4.670	1.0×10^{-14}	95.4	76.1	38.24	0.12		
1,500	30.10	0.0037	3.240	1.5×10^{-14}	96.8	92.9	38.34	0.11		
1,750	40.32	0.0045	37.47	6.3×10^{-15}	72.5	100	38.48	0.26		
Total gas age n = 16				9.0×10^{-14}			38.40	0.28		

L# = lab indentification number, NM and NMUM = irradiation package identification
[1] Blank corrected
[2] Corrected for ^{37}Ar decay
[3] Entry of (—) indicates no detectable ^{37}Ar due to long hiatus between irradiation and analysis

		Kinetic data		
Irradiation	Facility	$(^{36}Ar/^{37}Ar)_{Ca}$	$(^{39}Ar/^{37}Ar)_{Ca}$	$(^{40}Ar/^{39}Ar)_K$
NMUM-1	Univ. Michigan	0.00026 ± 2	0.00067 ± 3	0.018 ± 1
NM-13	Univ. Michigan	0.00026 ± 2	0.00070 ± 5	0.022 ± 1
NM-20	Univ. Michigan	0.00026 ± 2	0.00070 ± 5	0.019 ± 1
NM-23	Univ. Michigan	0.00025 ± 2	0.00070 ± 5	0.021 ± 3
NM-30	Univ. Michigan	0.00026 ± 2	0.00070 ± 5	0.021 ± 2
NM-38	Texas A&M	0.00026 ± 2	0.00070 ± 5	0.0002 ± 3

1988; Lo and Onstott, 1989). Following this rationale, we suggest that the total gas age best approximates the argon closure age, thus we infer an apparent age of 95.5 ± 1.1 Ma for sample 3 biotite.

The age spectrum for sample 4 primary hornblende is characterized by an overall saddle shape (Fig. 7c). Isochron analysis yields a linear array (MSWD = 5.5) with an apparent age of 95.2 ± 0.6 Ma and a trapped initial argon component of 311.0 ± 4.6 (Fig. 8b). The isochron age is considered to be the apparent age of sample 4 hornblende.

Sample 5 primary biotite yields a slightly complex age spectrum, but the final three heating steps which comprise ~65 percent of the total ^{39}Ar released define a plateau age of 91.9 ± 0.6 Ma (Fig. 7d). This plateau age is interpreted to be the apparent age of sample 5 biotite. This age is concordant with the hornblende and biotite ages previously published for the Osgood Mountains stock (Silberman et al., 1974)

Analyses of two sericites (samples 1 and 5) from silicified and gold-mineralized (stage 3) igneous rocks yield variably complex results. X-ray mapping reveals that the sericite occurs as plates within chlorite (Fig. 4). The chlorite variably replaces biotite on a hand-specimen scale as some biotites are very pristine, whereas others have been completely replaced. Figure 4 illustrates a portion of a chlorite grain which contains the 5- to 10-μm-thick by 50- to 150-μm-long sericite grains. The elemental maps clearly show that the high K regions do not contain Mg or Fe, thereby confirming that the high K needles are not remnant biotite phenocrysts from the Osgood Mountain stock. The sericite was not physically separated from the chlorite, but because it represents the only K-bearing phase within the large chlorite grains, the argon analysis will date the sericite. Sample 1 sericite yields an age spectrum with a plateau age of 83.1 ± 1.1 Ma for ~90 percent of the ^{39}Ar released (Fig. 7a). The final steps are significantly younger than the plateau age, and thus the total gas age of 82.3 ± 1.1 Ma is somewhat younger but not analytically distinct from the plateau age. Sample 5 sericite has a complex age spectrum (Fig. 7d) and does not yield a plateau age or a simple isochron relationship. The complexity may be related to ^{39}Ar recoil, and we suggest that the total gas age of 81.2 ± 1.5 Ma best approximates the apparent age of sample 5 sericite and also note that this age is indistinguishable from the plateau age of sample 1 sericite.

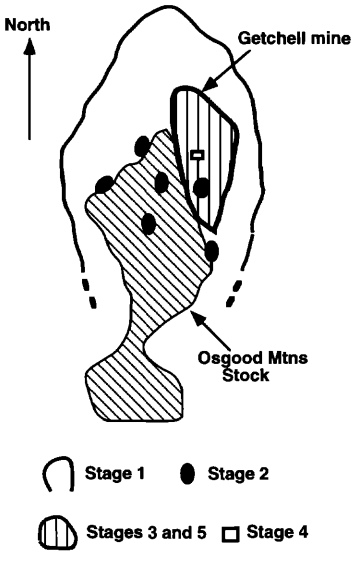

FIG. 6. Diagram showing the distribution, in plan view, of stages 1 to 5 mineralization in the northern Osgood Mountains. Mineralization generally occurs in localized pods and discrete breccia pipes. The most economically important stages 3 and 5 gold mineralization is located along the northeastern margin of the Osgood Mountains stock.

Several secondary K feldspar samples (1, 4, and 5) associated with stage 3 mineralization were analyzed (Table 2). The secondary K feldspar from samples 1 and 5 occurs as overgrowths and replacements of plagioclase (Fig. 5). At least two generations of K-feldspar are shown in the electron microprobe results where two compositionally distinct phases rim a large plagioclase grain. The age spectra for this secondary K feldspar is characterized by relatively young ages for the initial 5 to 10 percent of ^{39}Ar released and an undulatory pattern for the remainder of the age spectra (Fig. 7a, d). Ages of heating steps for this K feldspar rise to ~80 and 83 Ma, respectively, before decreasing in age to between 75 to 78 Ma (Fig. 7a, d). These complex age spectra are not readily explained by isochron analysis and may result from a combination of problems, such as, inhomogeneously distributed excess argon, ^{39}Ar recoil, a mixture of plagioclase and K feldspar from incomplete replacement of the plagioclase, and/or partial argon loss caused by younger thermal events. Secondary K feldspar from sample 4 has an age spectrum similar in form to those of samples 1 and 5 K feldspar but is significantly older, having apparent ages in the saddle portion of the spectrum ranging from ~82 to 84 Ma (Fig. 7c). An isochron age of 84.3 ± 0.9 Ma is given by ~90 percent of the ^{39}Ar released (Fig. 8c). This isochron age is taken to be the apparent age of this sample. The oldest ages associated with the highest temperature increments could reflect remnants of the original plagioclase grains (note drop in K/Ca for these steps, Fig. 7c) and/or excess ^{40}Ar. The overall low K/Ca (Fig. 7c) for this sample is probably related to incomplete replacement of plagioclase by secondary K feldspar.

Age spectra for samples 8 and 9 adularia (Fig. 7e) are flat and give plateau ages of 41.90 ± 0.25 and 42.11 ± 0.43 Ma. Sample 10 adularia yields a flat age spectrum with a plateau age of 38.26 ± 0.24 Ma (Fig. 7e).

K Feldspar Thermochronology

Unlike hydrous minerals, K feldspar remains relatively stable during heating in the ultra high vacuum system required for $^{40}Ar/^{39}Ar$ analysis. Therefore, age spectrum analysis of K feldspar has the potential to reveal the spatial distribution of ^{40}Ar within the crystal as well as an estimate of the argon retentivity which is derived from the laboratory kinetic parameters. Coupling the age spectrum and kinetic information can yield a quantitative thermal history for the sample and thus aid in placing all of the apparent ages determined by the $^{40}Ar/^{39}Ar$ technique into a thermochronologic framework.

Detailed thermochronologic analyses were performed on K feldspar of samples 6 and 7. As an attempt to acquaint the reader with the K feldspar methodology, a brief description of the technique precedes presentation of the discussion. Argon closure in K feldspar is treated on an individual sample basis by extending the closure temperature theory developed by Dodson (1973) to the multiple diffusion domain model of

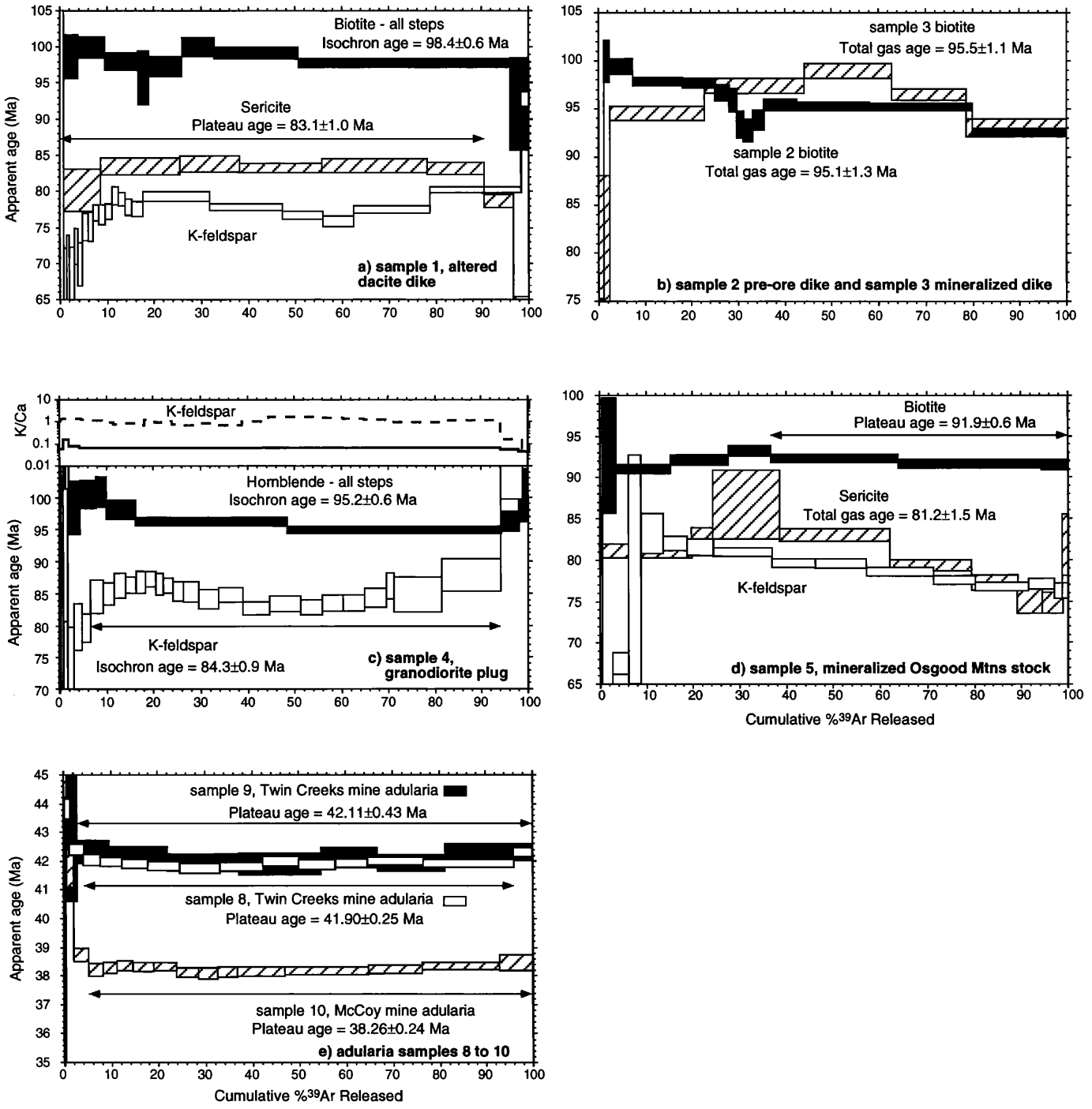

FIG. 7. $^{40}Ar/^{39}Ar$ age spectra. a. Sample 1—stage 3 gold mineralized dacite dike from the North pit, Getchell mine. Biotite is a primary phenocryst and sericite and secondary K feldspar represent stage 3 and stage 4(?) alteration of biotite and plagioclase, respectively. b. Sample 2—primary biotite from a dacite dike which contains stage 1 pyrrhotite collected at the Turquoise Ridge pit in the Getchell mine and sample 3—hydrothermal biotite from an Ordovician basalt which contains the stage 1 assemblage of pyrrhotite-chalcopyrite-arsenopyrite-biotite located on the Getchell property ~4 km northwest of the Main pit. c. Sample 4—primary hornblende from a argillized granodiorite plug and secondary K feldspar (after plagioclase) spatially associated with stage 3 mineralization located ~3 km east of the Main pit. d. Sample 5—primary Osgood Mountains stock biotite and stage 3 sericite and K feldspar from the Main pit, Getchell mine. e. Samples 8 and 9—stage 5 vein adularia from the Twin Creeks mine and sample 10 vein adularia from the McCoy mine.

Lovera et al. (1989). This model views K feldspar as containing a discrete distribution of domains with different argon diffusion length scales, which imparts multiple argon closure temperatures within a single sample. Because of this domainal nature for K feldspar, a continuous record of the thermal history, typically between about 150° to 350°C, may

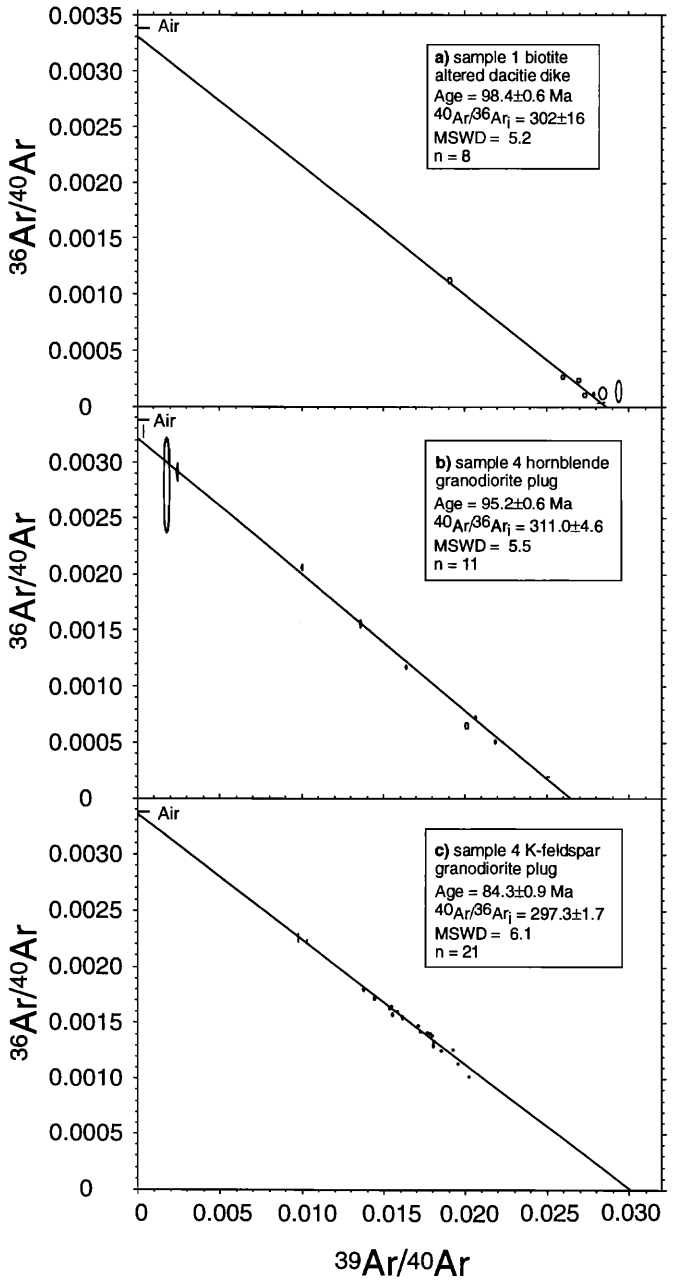

FIG. 8. Isochron diagrams for selected samples from the Getchell Mine area. The age is proportional to the x axis intercept and the trapped component (initial argon) is given by the y axis intercept. Each isochron suggests relatively minor excess argon ($^{40}Ar/^{36}Ar_i > 295.5$) and is probably the primary explanation for the moderate age spectrum complexity for these samples. The moderately high MSWD (goodness of fit parameter) is related to data scatter which is larger than that attributed solely to analytical error and may indicate a mixture of both atmospheric and excess initial argon. Sample information is given in the text and in the caption for Figure 7.

be recorded within one sample. That is, small diffusion domains will provide information about the low-temperature history, and the higher temperature history will be recorded by the larger diffusion domains.

Because the closure temperatures for K feldspar can be indirectly determined from the release of ^{39}Ar in the laboratory, extracting meaningful thermal histories from K feldspar argon results relies on the fundamental assumption that the release of argon in the laboratory occurs by the same mechanism and is controlled by the same boundaries, as in nature. Many studies confirm a good correlation between the argon kinetics derived using the multiple diffusion domain method and age spectra for most basement K feldspars (e.g., Lovera et al., 1989; Harrison et al., 1992; Leloup et al., 1993; Lee, 1995; Hoisch et al., 1997).

Argon diffusion coefficients, assuming a plane slab geometry, were determined for samples 6 and 7 K feldspar from the ^{39}Ar released in conjunction with the laboratory heating schedule and are displayed on an Arrhenius plot (Fig. 9). The activation energy (E) for each sample was obtained from the slope of the initial diffusion coefficients. Isothermal duplicate temperature steps were conducted to measure the reproducibility of individual diffusion coefficients at each temperature step (Table 2). Systematic separation of diffusion coefficients for isothermal steps indicates simultaneous degassing of more than one diffusion domain which would lead to an underestimation of the activation energy (Heizler and Harrison, 1991). The overall pattern of diffusion coefficients on the Arrhenius plot (Fig. 9) is a reflection of the variation in length (ρ) and volume faction (ϕ) of the diffusion domains. The kinetic parameters (Table 3) for each sample were obtained by applying the apparent activation energy and modeling the Arrhenius results as a distribution of diffusion domains (Lovera et al., 1989).

The log (r/r_o) plots shown in Figure 9 are a graphic method which displays the diffusion coefficient relative to the amount of ^{39}Ar contained within an Arrhenius data point. The advantage to this diagram over the Arrhenius plot is the relative ease of visualization of the volume fraction of diffusions domains. The log (r/r_o) diagram is derived by comparing the measured diffusion coefficients to a reference Arrhenius law. The reference Arrhenius law for each sample is defined by the initial linear segment on the Arrhenius plot and shown by the dashed lines in Figure 9. The value r_o is the diffusion length associated with the reference Arrhenius law, and r represents the length scale necessary to account for the deviation from this reference line. The log (r/r_o) values are only shown for laboratory extraction steps at or below 1,100°C since the sample begins to melt incongruently above this temperature. Finally, using the model kinetic parameters, the thermal history is retrieved by repeated forward modeling of the age spectrum.

The K feldspar age spectrum (Fig. 10a) from sample 7 reveals an age gradient from ~60 to 70 Ma to 90 Ma for the first 75 percent of gas released. The older apparent ages for the final 15 percent of the age spectrum are considered to result from excess argon contamination. Isochron analyses (not shown) for the three anomalously old steps yield an age of 95 ± 4 Ma, which overlaps the known age of the Osgood Mountains stock. The measured age spectrum can be readily modeled using the thermal histories shown in Figure 10. Rapid cooling to at least ~130°C is required to close the most retentive portion of the sample at 92 to 90 Ma. The age gradient revealed on the age spectrum can be modeled with either slow cooling from 125° to 80°C between ca. 90 to 75 Ma or a low-temperature thermal event at ~75 Ma (Fig. 10a). A thermal event subsequent to 90 Ma could not have exceeded ~125° to 150°C (depending upon the duration cho-

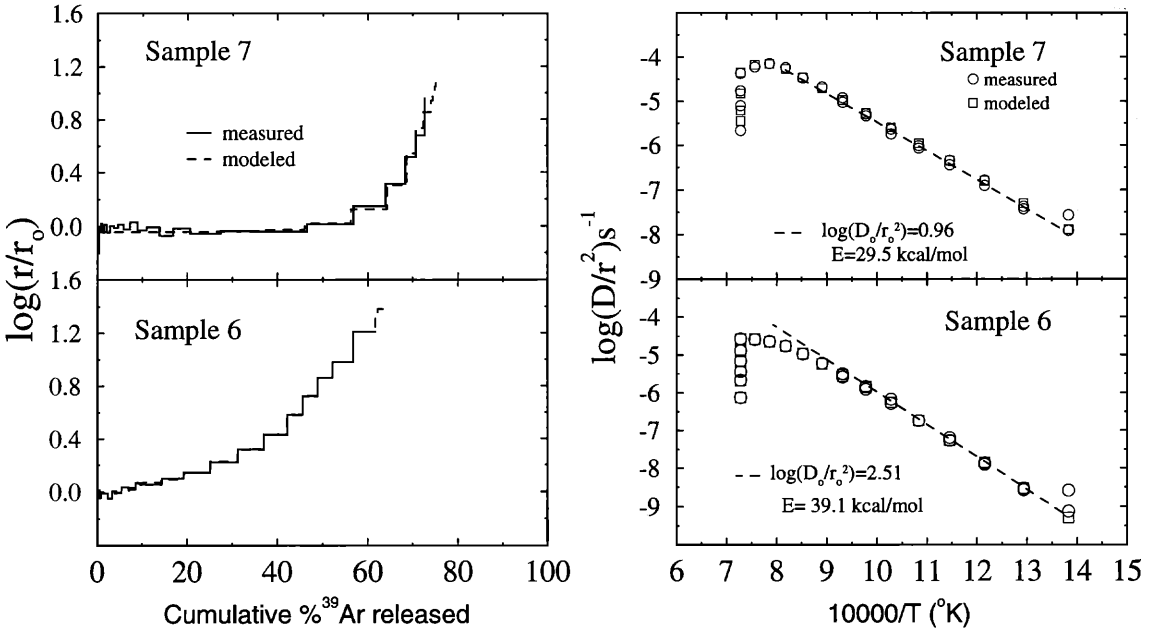

FIG. 9. Log (r/r_o) and Arrhenius plots for K feldspar samples 6 and 7. The dashed line on the Arrhenius diagram represents the reference Arrhenius law (activation energy (E) and log D_o/r_o^2) used to construct the log (r/r_o) plots. The low E for sample 7 yields an unusually low argon closure temperature (~135°C) for this sample but is consistent with the argon loss observed in the first 30 percent of the age spectrum of sample 7 K feldspar. Sample 6 yields a significantly higher E and directly corresponds to overall higher argon closure temperatures (Table 3) for each diffusion domain. The log (r/r_o) diagrams only show diffusion data calculated for argon loss associated with laboratory heating steps at or below 1,100°C due to the melting of the sample at higher laboratory extraction temperatures.

sen) since this would result in substantial argon loss, thereby partially or wholly resetting the K feldspar age at the time of the event. For the slow-cooling scenario, the age gradient can be modeled by linearly decreasing the temperature from 125° to 80°C between 90 and 75 Ma (Fig. 10a, b).

Sample 6 K feldspar (Fig. 10c, d) yields an age spectrum similar to that of sample 7 K feldspar, despite the fact it has significantly higher argon closure temperatures (Table 3). The measured age gradient for this K feldspar can be modeled with a thermal history envoking slow cooling from 300°C at 92 Ma to below 175°C by 75 Ma. Alternatively, the age spectrum can be modeled with a thermal history characterized by rapid cooling from 92 Ma to below 200°C by 90 Ma, followed with a short duration (~0.1 m.y.) thermal event of 250°C at 75 Ma (Fig. 10c, d). These examples illustrate that if reheating is a geologically viable thermal history, the multiple diffusion domain method cannot always provide a unique model. Therefore the thermal models must be interpreted in the context of the geologic relationships and style of mineralization and with respect to each other, in order to determine an accurate thermal history for either sample.

TABLE 3. Kinetic Parameters Used for K Feldspar Multiple Diffusion Domain Analysis

	Sample 6	Sample 6 T_c	Sample 7	Sample 7 T_c
E (kcal/mo)	39.1		29.5	
Log (D/r_1)	4.76	172	1.37	134
ϕ_1	0.0173		0.431	
Log (D/r_2)	3.57	200	1.36	134
ϕ_2	0.1046		0.156	
Log (D/r_3)	2.89	217	1.34	135
ϕ_3	0.1785		0.072	
Log (D/r_4)	2.43	230	0.34	168
ϕ_4	0.1095		0.075	
Log (D/r_5)	1.53	257	−2.04	237
ϕ_5	0.1365		0.266	
Log (D/r_6)	−0.49	328		
ϕ_6	0.4536			

E is activation energy, ϕ is volume fraction, r is diffusion length, and T_c is closure temperature (°C)

Discussion

Timing of gold mineralization

The interpretation of the combined results from studies of mineral paragenesis, geologic relationships, and $^{40}Ar/^{39}Ar$ geochronology can be synthesized to provide a coherent, composite, five-stage mineralization history for the Getchell and Twin Creeks deposits (Table 4). A fundamental conclusion from the $^{40}Ar/^{39}Ar$ data is that the region did not experience protracted elevated temperatures at deep crustal levels during the Cretaceous or Tertiary. Several lines of evidence indicate that the Getchell trend developed at shallow crustal levels, and that heating events related to igneous intrusions, particularly the Osgood Mountains stock, were relatively brief and localized. Support for this comes from several sources: K feldspar thermochronology, discussed below, shows that the Osgood Mountains stock cooled to less than 125°C within 2 m.y. of emplacement; concordant hornblende and biotite K/Ar ages from the Osgood Mountains stock and a nearby andesite dike (Silberman et al., 1974; Berger and Taylor, 1980) indicate rapid cooling from ~500° to 300°C; miarolitic cavities in porphyry dikes (Hotz and Wilden, 1964); and a

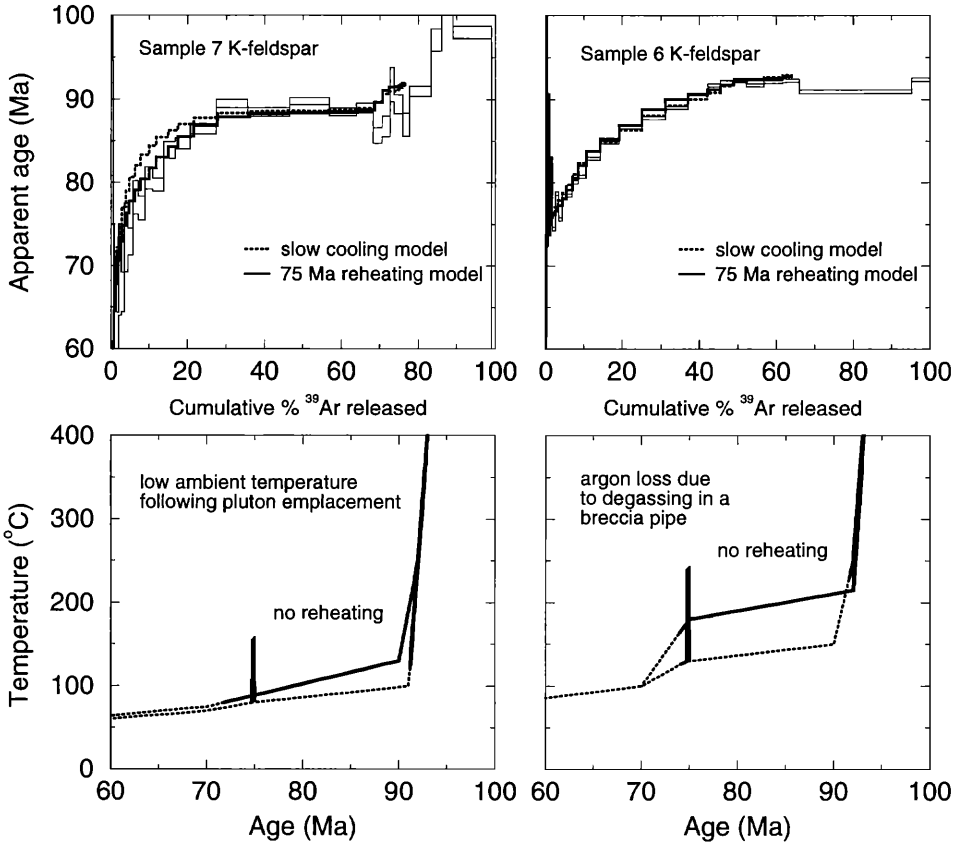

FIG. 10. Measured and model age spectra and calculated thermal histories for K feldspar samples 6 and 7. The solid lines on the time-temperature diagrams represent the portions of the model thermal history which can be constrained by the measured age spectra and argon kinetic properties, whereas the dashed segments are inferred and not constrained by the measured data. Model age spectra which well approximate the measured age spectra can be calculated using either slow cooling or episodic reheating, although each model requires ambient temperatures below about 130° to 150°C since the Cretaceous. As discussed in the text, sample 6 records the time of argon loss in the K feldspar due to thermal degassing caused by incorporation of the clast in the breccia pipe at ca. 75 Ma. The low argon closure temperature of sample 7 K feldspar allows for argon loss associated with a minor thermal perturbation atc ~75 Ma and/or diffusive argon loss in conjunction with ambient temperatures of about 100°C.

geobarometrically calculated pressure of 1.5 kbars (~4–6 km) for the emplacement of the Osgood Mountain stock (Taylor, 1976) all indicate shallow crustal levels.

Because of overwhelming evidence for shallow crustal levels, low ambient temperatures, and consequent rapid cooling of igneous intrusions, $^{40}Ar/^{39}Ar$ ages are interpreted to give the direct dates of thermal events related to mineralization and not simply the apparent ages reflecting protracted cooling.

Stage 1 skarn mineralization—95 Ma

The initial mineralizing event on the Getchell property occurred after igneous activity at 98 Ma and is represented by stage 1 pyrrhotite-arsenopyrite-chalcopyrite-biotite ± gold mineralization in skarn. The first phase of igneous activity on the Getchell property is documented by an age of 98.4 ± 0.6 Ma for sample 1 biotite from a dacitic dike (Fig. 7a). A second phase of igneous activity is evidenced by an age of 95.1 ± 0.7 for sample 2 biotite from a pyrrhotite-rich dacite dike and an age of 95.2 ± 0.6 Ma for sample 4 hornblende from a granodiorite plug (Fig. 7b, c). Based on these biotite and hornblende ages, at least two discrete periods of igneous activity occurred prior to the emplacement of the ~92 Ma Osgood Mountains stock. Stage 1 mineralization also occurred before the emplacement of the Osgood Mountains stock, based on an age of 95.5 ± 1.1 Ma for a hydrothermal biotite from sample 3 (Fig. 7b).

Stage 2 skarn mineralization—92 Ma

Chalcopyrite-galena-sphalerite-silver-sericite (?) ± gold mineralization in skarns at the Getchell and Twin Creeks deposits could not be directly dated by $^{40}Ar/^{39}Ar$ methods but is related to the Osgood Mountains stock based on geologic relationships and published K/Ar results. Base metal mineralization in the Osgood Mountains region is contained in the skarn that formed during the emplacement of the Osgood Mountains stock or as quartz-base metal veins in the stock. At the north end of the Twin Creeks mine, base metal veins within envelopes of sericitic alteration are in close proximity to two granodiorite dikes (Osterberg, 1989). A 92.1 Ma sericite age was reported by Osterberg (1989) from the north end of the Twin Creeks mine and presumably dates the sericitic alteration. Sericite K/Ar ages of ~92 Ma were also reported by Silberman et al. (1974) for tungsten mineralization in skarn adjacent to the Osgood Mountains stock and within altered

TABLE 4. $^{40}Ar/^{39}Ar$ Chronology Summary

Time (Ma)	Event	Preferred sample ages (Ma)
98	Emplacement of dacitic dike	Sample 1 biotite 98.4 ± 0.6
95	Stage 1 mineralization, emplacement of igneous intrusions	Sample 2 biotite 95.1 ± 0.7 Sample 3 biotite 95.5 ± 1.1 Sample 4 hornblende 95.2 ± 0.6
92	Stage 2 mineralization, emplacement of Osgood Mts. stock	Sample 5 biotite 91.9 ± 0.6
83	Stage 3 mineralization	Sample 1 sericite 83.1 ± 1.1 Sample 5 sericite 81.2 ± 1.5 Sample 4 K feldspar 84.3 ± 0.9
75	Stage 4 mineralization	Sample 1, sample 5, sample 6 K feldspar argon loss at 75
42	Stage 5 mineralization	Sample 8 adularia 41.90 ± 0.25 Sample 9 adularia 42.11 ± 0.43

areas of the stock. We interpret these geologic relationships and K/Ar ages to indicate that stage 2 base metal mineralization occurred shortly after the emplacement of the Osgood Mountains stock.

Stage 3 Carlin-type mineralization—83 Ma

The major gold mineralizing event on the Getchell property is represented by stage 3 quartz-pyrite-kaolinite-sericite-gold mineralization. The timing of this economically important gold event has never been clearly documented and is the subject of considerable debate. Silberman et al. (1974) argued that gold mineralization was related to the Osgood Mountains stock based on the close spatial association between the stock and gold mineralization and sericite K/Ar dates for tungsten mineralization which overlap with the age of the stock. In contrast, Joralemon (1951) proposed that gold was deposited in a hot spring environment and was related to Tertiary rhyolitic tuffs at the North pit, Getchell mine. The more recent discovery of additional gold deposits in the district (e.g., Twin Creeks), distal to the Osgood Mountains stock, further complicates interpretations of the genetic association between the exposed igneous rocks and Carlin-type gold mineralization.

Thin section analyses of stage 3 mineralized igneous rocks at the Getchell mine indicate that a K-rich phase of alteration accompanied this economically important gold event. Samples of sericite and secondary K feldspars, from stage 3 mineralized rocks, yield apparent ages of ~83 and ~75 to 78 Ma, respectively (Fig. 7a, d; Table 4). In order to interpret the geologic significance of this age discordance, and to determine if stage 3 mineralization is related to the Osgood Mountains stock, the thermal evolution of the area must be known. For instance, these stage 3 ages could represent growth of new phases during mineralization unrelated to the Osgood Mountains stock, or argon loss caused by discrete thermal event(s) and/or slow cooling. With this in mind, we now turn to a discussion of the thermal history analysis before interpreting the geologic significance of the stage 3 sericite and secondary K feldspar apparent ages.

Thermochronology

The thermal history of the area can be obtained from age determinations on cogenetic minerals which have different argon closure temperatures and K feldspar multiple diffusion domain results. As previously discussed, the concordant hornblende-biotite K/Ar ages of 91.7 ± 1.8 and 94.5 ± 1.8 Ma (Silberman et al., 1974) indicate rapid cooling from 500° to 300°C for the Osgood Mountains stock. This rapid, high-temperature, cooling history is corroborated by Berger and Taylor (1980) who report concordant hornblende-biotite K/Ar ages of 91.9 ± 1.8 and 91.7 ± 1.8 Ma for an andesite dike at the Getchell mine.

The low-temperature (~100°–300°C) thermal history can be interpreted from the K feldspar results. Recall that samples 6 and 7 K feldspar were modeled using the multiple diffusion domain method and yielded age spectra characterized by age gradients for the first 30 to 40 percent argon released followed by relatively flat portions (92–90 Ma) for the remainder of gas released (Fig. 10). These measured age spectra can be modeled with thermal histories envoking either slow cooling or episodic argon loss related to a younger reheating event (Fig. 10). Multiple diffusion domain modeling of sample 7 K feldspar requires cooling to 125°C by 90 Ma in order to close the most retentive portion of the sample. Regardless of the choice of a slow cooling model or a reheating model, the sample could not have been maintained or reheated above about 150°C since 90 Ma and must have cooled below ~80°C by 75 Ma. This lowest temperature portion of the K feldspar thermal history is consistent with the available fission track data from the Osgood Mountains stock. Apatite fission track ages for samples collected distant from the Getchell fault yield apparent ages of 70 to 80 (± 10) Ma (C.W. Naeser, pers. commun., 1991), suggesting cooling of the stock below ~80°C by 80 to 70 Ma. Older fission track ages (90–80 ± 10 Ma) for zircon and sphene (C.W. Naeser, pers. commun., 1991) are also compatible with the K feldspar determined thermal history.

Sample 6 K feldspar, a pegmatitic clast in a mineralized breccia pipe, has an age spectrum (Fig. 10c) very similar tothat of sample 7 but overall has much higher argon closure temperatures. The ca. 92 Ma plateau portion for sample 6 K feldspar records the time of cooling to below 350°C and indicates that sample 6 represents a pegmatitic phase of the Osgood Mountains stock. The age spectrum and argon kinetics permit a model in which sample 6 cools slowly to 175°C from 92 to 75 Ma. This model is not preferred because its high temperatures are inconsistent with the thermal history given by sample 7 K feldspar. On the other hand, the thermal history incorporating an episodic reheating event is entirely consistent with the geologic and mineralogic setting of this sample. The pegmatitic K feldspar clasts are encompassed in a siliceous matrix which contains fine-grained auriferous pyrite. Fluid inclusion data for mineralization in the breccia pipe indicate temperatures of ~250°C (Groff, 1996), consistent with the clasts being heated to this temperature upon incorporation into the pipe. The age spectrum and thermal history for sample 6 and the low ambient temperature required for sample 7 indicate that breccia pipe intrusion and associated reheating occurred at ~75 Ma (Fig. 10c, d).

In summary, the thermal histories indicated by K feldspar samples 6 and 7 are geologically reasonable and consistent with other thermochronometers. Sample 7 clearly indicates that the sample area has been relatively cool (~80°–150°C) since 90 Ma. Any mineralizing fluids or intrusions emplaced

during this period would quickly cool to these ambient temperatures. Consequently, if minerals, with closure temperatures greater than about 150°C were precipitated, their ages would record the timing of the mineralizing event.

With knowledge gained from the thermal history analysis presented above, it is clear that stage 3 mineralization occurred at relatively shallow depths and that protracted cooling following the emplacement of the Osgood Mountains stock is not reasonable. Therefore, the age discordance between 98 to 92 Ma primary biotites and 83 to 81 Ma coarse-grained sericite replacements, in stage 3 samples 1 and 5, is a consequence of sericite mineral growth during stage 3 mineralization at ~83 Ma. The fact that the biotites from stage 3 sericitized samples 1 and 5 retain their primary ages is consistent with fluid temperatures of 200° to 250°C for quartz-pyrite-gold mineralization in Carlin-type deposits (Hofstra et al., 1989; Kuehn, 1989; Osterberg, 1989; Groff, 1996). That is, if much higher temperatures (~300°C) occurred in association with stage 3 mineralization, we would expect the biotites to be partially or wholly reset. This also implies that sericite precipitation occurred at or below 250°C. Therefore, based on thermochronologic results and geologic relationships at the Getchell deposit, it is clear that gold mineralization in stage 3 is not temporally associated with the intrusion of the 92 Ma Osgood Mountains stock but rather occurred as a discrete event at 83 Ma.

Stage 4 breccia pipe mineralization—75 Ma

Stage 4 mineralization is characterized by low-grade quartz-pyrite-gold mineralization associated with the emplacement of two breccia pipes that cut high-grade stage 3 ores in the Getchell underground. The multiple diffusion domain modeling of K feldspar from sample 6, described in the previous section, indicates an age of 75 Ma for the breccia pipe and associated stage 4 mineralization. This ca. 75 Ma event may help to explain why apparently cogenetic secondary K feldspar and sericite record apparent ages of 78 to 75 and 83 to 81 Ma, respectively. This 5 to 8 m.y. age discordance could be recording a discrete interval of K feldspar growth at ca. 75 Ma with the age spectrum complexity (Fig. 7a, d) resulting from a mixture of two age discordant populations. The electron microprobe analyses clearly indicate two K feldspar populations, presumably one dating at ~83 Ma and one at ~75 Ma. Clearly, we have no direct measure of the age of each population, but since stage 3 is shallow (~2 km; Groff, 1996), slow cooling does not appear to be a viable mechanism to explain this age discordance between the sericite and bulk secondary K feldspar results.

The distribution of K feldspar ages in the area of the Getchell mine suggests that the ~75 Ma stage 4 mineralization was restricted to the Getchell fault zone. The secondary K feldspar samples with 75 to 78 Ma ages were obtained from the fault zone itself. Sample 4, located ~3 km east of the Getchell fault zone, has an isochron age of 84.3 ± 0.9 Ma, identical to stage 3 sericite ages. The diffusion coefficients (Table 2) of this sample indicate that temperatures remained below 170°C after 84 Ma. Sample 7 suggests that temperatures at 75 Ma were less than 150°C (Fig. 10b) at distances of ~2 km west of the Getchell fault zone.

Stage 5 Carlin-type mineralization—42 Ma

Stage 5 ores from the Getchell and Twin Creeks mines consist of stibnite-orpiment-pyrite-gold ± realgar. Where stage 5 overprints stage 3 mineralization, higher gold grades are recognized. Adularia from the Twin Creeks mine was dated to determine the precise age of stage 5 mineralization. Samples 8 and 9 adularia yield indistinguishable apparent ages of 41.90 ± 0.25 and 42.11 ± 0.43 Ma (Fig. 7e), much younger than the Cretaceous stage 1 to 4 events. These adularia samples apparently grew below their relatively high closure temperature (>300°C for sample 9, based on the Arrhenius parameters) and thus directly date stage 5 mineralization. The timing of stage 5 at the Getchell mine could not be directly determined because adularia was not identified with orpiment and stibnite mineralization. However, fission track dating of apatites from the Getchell mine yields relatively young apparent ages of 52 to 35 (±10) Ma near orpiment-pyrite-stibnite-gold and realgar mineralization in the Getchell fault (C.W. Naeser, pers. commun., 1991). These young apparent apatite ages probably reflect partial fission track annealing because temperatures of 100° to 160°C were documented by fluid inclusion microthermometry for the orpiment-realgar mineralization in the Getchell fault (Groff and Norman, 1993). Indirect evidence for stage 5 mineralization occurring at about 42 Ma at the Getchell mine is therefore provided by the $^{40}Ar/^{39}Ar$ adularia ages from the Twin Creeks mine and the fission track dating for granodiorite in close proximity to orpiment and realgar mineralization in the Getchell fault.

A compilation of all the gold mineralizing and igneous events and the interpreted thermal history for the Getchell deposit is given in Figure 11. This probability distribution diagram depicts our interpretation that the low-temperature ambient conditions, revealed by the K feldspar thermochronometric results, were periodically punctuated by high-temperature mineralizing and igneous events. The ages of the events are clearly distinguishable outside the analytical error of the age determinations.

Regional Implications

The formation of the Carlin-type orebodies at the Getchell and Twin Creeks mines was the result of the overprinting of gold mineralizing events at 83 and 42 Ma. Cretaceous gold mineralization in Carlin-type deposits along the Getchell, Carlin, and Battle Mountain-Eureka trends is supported by age determinations for sericites that replace primary biotite in mineralized igneous rocks. A Cretaceous gold mineralizing event at the Post-Betze mine, Carlin trend, was suggested by Arehart et al. (1993b) based on an interpreted age of 117 Ma for hydrothermal sericites from gold-mineralized portions of the Goldstrike stock. At the nearby Carlin mine, $^{40}Ar/^{39}Ar$ ages of 123 to 120 Ma are recorded by sericite that replaces biotite in an altered dike (Kuehn, 1989). A Cretaceous gold event at the Gold Acres mine, Battle Mountain-Eureka trend, is consistent with 92.8 ± 1.0 Ma sericite formed by the alteration of a 99.8 ± 1.2 Ma granite pluton, and with an altered quartz-porphyry dike in the mine that contains 94.3 ± 1.9 Ma sericite (Wrucke and Armubrustmacher, 1975). Cretaceous gold mineralization for the Battle Mountain-Eureka, Carlin, and Getchell trends could be associated with episodic

Cretaceous igneous activity at these localities (Theodore et al., 1973; Silberman et al., 1974; Erickson et al., 1978; Radtke, 1985).

Age data from gold-rich skarn and Carlin-type deposits along the Battle Mountain-Eureka, Carlin, and Getchell trends are consistent with a regional mineralizing event in the Eocene. The age of gold and base metal mineralization in skarns along the Battle Mountain-Eureka trend is 38.24 ± 0.24 Ma as determined by sample 10 adularia (Fig. 7e), which is associated with quartz-pyrite-gold mineralization in skarn at the McCoy mine. Also, zonation of gold and base metal mineralization around a 38.5 Ma granodiorite stock (Theodore et al., 1973) at the Fortitude mine suggests mineralization in the Eocene.

In contrast to the skarn and base metal deposits, the age of Carlin-type gold mineralization in deposits along the Battle Mountain-Eureka and Carlin trends has yet to be clearly documented. However, an Eocene age for Carlin-type mineralization is suggested by several studies at various localities. Along the Battle Mountain-Eureka trend, Carlin-type gold mineralization at Tonkin Springs is bracketed by volcanic rocks dated at 37.5 ± 0.4 and 33.4 ± 2.6 Ma (Maher et al., 1993). An Eocene age for Carlin-type gold mineralization at the nearby Cortez mine is suggested by an altered 34 Ma porphyry intrusion proximal to ore (Wells et al., 1969). At the Post-Betze mine, Carlin trend, ages of 39.9 Ma for an altered sill and a 36 Ma postore dike bracket a possible Eocene gold mineralizing event (Bettles and Lauha, 1991; Arehart et al., 1993b). Additionally, quartz-adularia-gold stockworks at Tuscarora, dated at 38 Ma, may be related to mid-Tertiary igneous activity and gold mineralization along the Carlin trend (Roberts et al., 1971).

Eocene Carlin-type gold mineralization along the Battle Mountain-Eureka, Carlin, and Getchell trends may be a regional event related to Eocene volcanism. Recent work by Brooks et al. (1995) suggests that Eocene volcanism was widespread in northeast Nevada and Utah and is spatially associated with gold mineralization.

Conclusions

The Getchell and Twin Creeks deposits formed in an area of repeated episodes of igneous intrusions and multiple gold mineralizing events. Igneous intrusions at the Getchell deposit were emplaced at 98, 95, and 92 Ma. Gold mineralization occurred in five mineralogically and temporally distinct stages during the Cretaceous and Tertiary. Stage 1 pyrrhotite-arsenopyrite-chalcopyrite-biotite ± gold mineralization at 95 Ma and stage 2 chalcopyrite-galena-sphalerite-silver ± gold mineralization at 92 Ma represent skarn-gold events that preceded and are unrelated to Carlin-type mineralization. The first Carlin-type gold event is represented by stage 3 quartz-pyrite-kaolinite-gold mineralization, which formed at 83 Ma. Relatively minor stage 4 quartz-pyrite-gold mineralization at 75 Ma is located in the matrix of two breccia pipes that cut

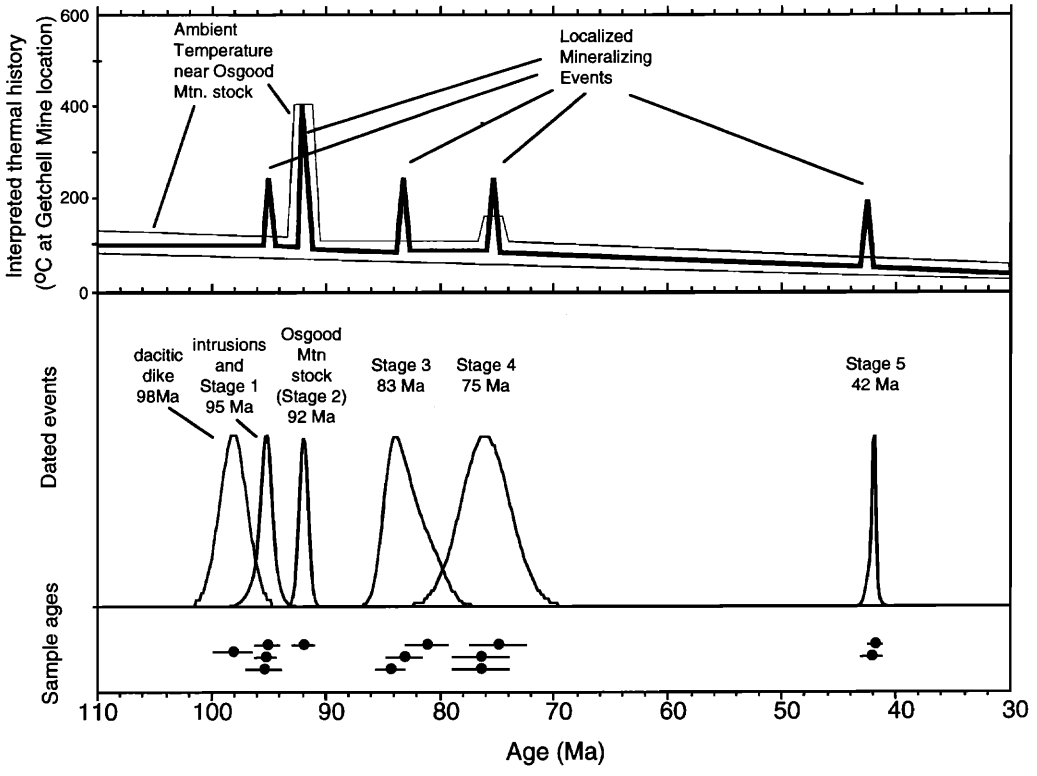

FIG. 11. Relative probability diagram representing the timing of igneous activity and gold mineralization in stages 1 to 5. The ages of individual samples are represented by the solid circles with associated 2σ error bars. The separation of the nodes indicate that individual events can be resolved outside the analytical error. The gray band is the ambient temperature near the Osgood Mountains stock determined mainly by the K feldspar thermal history and apatite fission track data. The low ambient temperature is punctuated by the high-temperature localized events associated with mineralization, as indicated by the thin black line within the gray band.

83 Ma stage 3 mineralization. The second Carlin-type gold event is represented by stage 5 orpiment-stibnite-pyrite-gold ± realgar mineralization, which formed at 42 Ma. The Carlin-type orebodies at the Getchell and Twin Creeks mines therefore formed as a result of the overprinting of 83 Ma quartz-pyrite-kaolinite-gold mineralization by 42 Ma orpiment-stibnite-pyrite-gold mineralization and are genetically unrelated to older skarn-gold mineralization in the district.

Acknowledgments

We would like to thank the Getchell Gold Corporation and Santa Fe Pacific Gold Corporation for access to the Getchell and Twin Creeks mines, respectively, and help with sampling. The understanding of these complex orebodies was greatly improved by lengthy discussions, of sometimes controversial data, with geologists at the Getchell and Twin Creeks mines. Funding for the age dating portion of this study was provided by a grant from the Geological Society of America, other support was provided by the mining companies. Electron microprobe analyses were conducted by Nelia Dunbar at the New Mexico Bureau of Mines and substantially clarified the complex mineralogy of stage 3. Constructive reviews by *Economic Geology* referees significantly improved the clarity of the manuscript and are greatly appreciated.

March 25, 1996; July 28, 1997

REFERENCES

Arehart, G.B., Chryssoulis, S.L., and Kesler, S.E., 1993a, Gold and arsenic in iron sulfides from sediment-hosted disseminated gold deposits: Implications for depositional processes: ECONOMIC GEOLOGY, v. 88, p. 171–185.

Arehart, G.B., Foland, K.A., Naeser, C.W., and Kesler, S.E., 1993b, $^{40}Ar/^{39}Ar$, K/Ar, and fission track geochronology of sediment-hosted disseminated gold deposits at Post-Betze, Carlin trend, northeastern Nevada: ECONOMIC GEOLOGY, v. 88, p. 622–646.

Bagby, W.C., and Berger, B.R., 1985, Geologic characteristics of sediment-hosted, disseminated precious-metal deposits in the western United States: Reviews in Economic Geology, v. 2, p. 169–202.

Bakken, B.M., Hochella, M.F., Jr., Marshall, A.F., and Turner, M.A., 1989, High-resolution microscopy of gold in unoxidized ore from the Carlin mine, Nevada: ECONOMIC GEOLOGY, v. 84, p. 171–179.

Berger, B.R., 1986, Descriptive model of carbonate-hosted Au-Ag: U.S. Geological Survey Bulletin 1693, p. 175.

Berger, B.R., and Taylor, J., 1980, Pre Cenozoic normal faulting in the Osgood Mountains, Humboldt County, Nevada: Geology, v. 8, p. 594–598.

Bettles, K.H., and Lauha, E.A., 1991, Gold deposits of the Goldstrike mine, Carlin trend, Nevada: World Gold '91, Australasian Institute of Mining and Metallurgy-Society of Mining Engineers Joint Conference, 2nd, Cairns, Australia, April 21–25, 7 p.

Brooks, W.E., Thorman, C.H., and Snee, L.W., 1995, The $^{40}Ar/^{39}Ar$ ages and tectonic setting of the middle Eocene northeast Nevada volcanic field: Journal of Geophysical Research, v. 100, p. 10,403–10,416.

Dodson, M.H., 1973, Closure temperature in cooling geochronological and petrological systems: Contributions to Mineralogy and Petrology, v. 40, p. 259–274.

Erickson, R.L., and Marsh, S.P., 1974, Paleozoic tectonics in the Edna Mountain quadrangle, Nevada: U.S. Geological Survey Journal of Research, v. 2, p. 331–337.

Erickson, R.L., Silberman, M.L., and Marsh, S.P., 1978, Age and composition of igneous rocks, Edna Mountain quadrangle, Humboldt County, Nevada: U.S. Geological Survey Journal of Research, v. 6, p. 727–743.

Groff, J.A., 1996, Geochronology and origin of auriferous fluids for the Getchell and Twin Creeks mines, Humboldt County, Nevada: Unpublished Ph.D. dissertation, Socorro, New Mexico Institute of Mining and Technology, 291 p.

Groff, J.A., and Norman, D.I., 1993, Mineral paragenesis and characteristics of fluids associated with mineralization in the Getchell and Twin Creeks mines, with reference to the Carlin mine, Nevada: Littleton, Colorado, Society of Mining, Metallurgy, and Exploration Preprint 94–77, 10 p.

Harrison, T.M., 1981, The diffusion of ^{40}Ar in hornblende: Contributions to Mineralogy and Petrology, v. 78, p. 324–331.

Harrison, T.M., Duncan, I.J., and McDougall, I., 1985, Diffusion of ^{40}Ar in biotite: Temperature, pressure, and compositional effects: Geochimica et Cosmochimica Acta, v. 49, p. 2461–2468.

Harrison, T.M., Chen, W., Leloup, P.H., Ryerson, F.J., and Tapponnier, P., 1992, An early Miocene transition in deformation regime within the Red River fault zone, Yunnan, and its significance for Indo-Asian tectonics: Journal of Geophysical Research, v. 97, p. 7159–7182.

Heizler, M.T., and Harrison, T.M., 1991, The heating duration and provenance age of rocks in the Salton Sea geothermal field, southern California: Journal of Volcanology and Geothermal Research, v. 46, p. 73–97.

Heizler, M.T., Lux, D.R., and Decker, E.R., 1988, The age and cooling history of the Chain of Ponds and Big Island Pond plutons and the Spider Lake Granite, west-central Maine and Quebec: American Journal of Science, v. 288, p. 925–952.

Hofstra, A.H., Northrop, H.R., Rye, R.O., Landis, G.P., and Birak, D.J., 1988, Genesis of sediment-hosted disseminated gold deposits by fluid mixing and sulfidization: Chemical reaction path modeling of ore deposition process documented at the Jerritt Canyon district, Nevada: Geology, v. 19, p. 36–40.

Hoisch, T.D., Heizler, M.T., and Zartman, R.E., 1997, Timing of detachment faulting west of Yucca Mountain, Nevada: Inferences from $^{40}Ar/^{39}Ar$, K-Ar, U-Pb, and fission-track thermochronology: Journal of Geophysical Research, v. 102, p. 2815–2833.

Hotz, P.E., and Wilden, R., 1964, Geology and mineral deposits of the Osgood Mountains quadrangle, Humboldt County, Nevada: U.S. Geological Survey Professional Paper 431, 128 p.

Hubacher, F.A., and Lux, D.R., 1987, The timing of Acadian deformation in northeastern Maine: Geology, v. 15, p. 80–83.

Ilchik, R.P., 1995, $^{40}Ar/^{39}Ar$, K/Ar, and fission track geochronology of sediment-hosted disseminated gold deposits at Post-Betze, Carlin trend, northeastern Nevada—a discussion: ECONOMIC GEOLOGY, v. 90, p. 208–210.

Joralemon, P., 1951, The occurrence of gold at the Getchell mine: ECONOMIC GEOLOGY, v. 46, p. 267–310.

Kuehn, C.A., 1989, Studies of disseminated gold deposits near Carlin, Nevada: Evidence for a deep geologic setting of ore formation: Unpublished Ph.D. dissertation, University Park, Pennsylvania State University, 395 p.

Lee, J., 1995, Rapid uplift and rotation of mylonitic rocks from beneath a detachment fault: Insights from potassium feldspar $^{40}Ar/^{39}Ar$ thermochronology, northern Snake Range, Nevada: Tectonics, v. 14, p. 54–77.

Leloup, P.H., Harrison, T.M., Ryerson, F.J., Wenji, C., Qi, L., Tapponnier, P., and Lacassin, R., 1993, Structural, petrological and thermal evolution of a Tertiary ductile strike-slip shear zone, Diancang Shan, Yunnan: Journal of Geophysical Research, v. 98, p. 6715–6743.

Lo, C.H., and Onstott, T.C., 1989, ^{39}Ar recoil artifacts in chloritized biotite: Geochimica et Cosmochimica Acta, v. 53, p. 2697–2711.

Lovera, O.M., Richter, F.M., and Harrison, T.M., 1989, The $^{40}Ar/^{39}Ar$ thermochronometry for slowly cooled samples having a distribution of diffusion domain sizes: Journal of Geophysical Research, v. 94, p. 17,917–17,935.

Madden-McGuire, D.J., Snee, L.W., and Smith, S.M., 1991, Age of alluvium adjacent to the Rabbit Creek gold deposit using $^{40}Ar/^{39}Ar$ age spectrum dating of biotite from reworked volcanic tuff, Humboldt County, Nevada, *in* Raines, G.L., Schafer, R.W., and Wilkinson, W.H., eds., Geology and ore deposits of the Great Basin Symposium proceedings: Reno, Nevada, Geological Society of Nevada, p. 324–334.

Madrid, R., 1987, Stratigraphy of the Roberts Mountain allocthon in north-central Nevada: Unpublished Ph.D. dissertation, Stanford, California, Stanford University, 346 p.

Maher, B.J., Browne, Q.J., and McKee, E.H., 1993, Constraints on the age of gold mineralization and metallogenesis in the Battle Mountain-Eureka mineral belt, Nevada: ECONOMIC GEOLOGY, v. 88, p. 469–478.

McIntosh, W.C., and Cather, S.M., 1994, $^{40}Ar/^{39}Ar$ geochronology of basaltic rocks and constraints on the late Cenozoic stratigraphy and landscape development in the Red Hill-Quemado area, New Mexico: Geological Society of New Mexico Field Conference, 45th, Socorro, New Mexico, Guidebook, p. 209–224.

Moore, W.J., and McKee, E.H., 1983, Phanerozoic magmatism and mineralization in the Tooele 1° × 2° quadrangle, Utah: Geological Society of America Memoir 157, p. 183–190.

Osterberg, M.W., 1989, Geology and geochemistry of the Chimney Creek gold deposit, Humboldt County, Nevada: Unpublished Ph.D. dissertation, Tucson, University of Arizona, 145 p.

Radtke, A.R., 1985, Geology of the Carlin gold deposit, Nevada: U.S. Geological Survey Professional Paper 1267, 124 p.

Roberts, R.J., 1964, Stratigraphy and structure of the Antler Peak quadrangle, Humboldt and Lander Counties, Nevada: U.S. Geological Survey Professional Paper 459-A, 93 p.

——1966, Metallogenic provinces and mineral belts in Nevada: Nevada Bureau of Mines and Geology Report 13, part A, p. 47–72.

Roberts, R.J., Radtke, A.R., and Coats, R.R., 1971, Gold-bearing deposits in north-central Nevada and southwestern Idaho: With a section on plutonism in north-central Nevada by Silberman, M.L., and McKee, E.H.: ECONOMIC GEOLOGY, v. 66, p. 14–33.

Rowell, A.J., Rees, M.N., and Suzcek, C.A., 1979, Margin of the North American continent in Nevada during late Cambrian time: American Journal of Science, v. 279, p. 1–18.

Samson, S.D., and Alexander, E.C., Jr., 1987, Calibration of the Interlaboratory $^{40}Ar/^{39}Ar$ dating standard, Mmhb-1: Chemical Geology, v. 66, p. 27–34.

Shawe, D.R., 1991, Structurally controlled gold trends imply large gold resource in Nevada, *in* Raines, G.L., Schafer, R.W., and Wilkinson, W.H., eds., Geology and ore deposits of the Great Basin Symposium proceedings: Reno, Nevada, Geological Society of Nevada, p. 199–212.

Shawe, D.R., and Nolan, T.B., 1989, Gold in the Eureka mining district, Nevada: U.S. Geological Survey Bulletin 1857-C, p. C29–C37.

Silberman, M.L., Berger, B.R., and Koski, R.A., 1974, K-Ar age relations of granodiorite emplacement and W and Au mineralization near the Getchell mine, Humboldt County, Nevada: ECONOMIC GEOLOGY, v. 69, p. 646–656.

Steiger, R.H., and Jager, E., 1977, Subcommission of geochronology: Convention on the use of decay constants in geo- and cosmochronology: Earth and Planetary Science Letters, v. 36, p. 359–362.

Taylor, B.E., 1976, Origin and significance of C-O-H fluids in the formation of Ca-Fe-Si skarn, Osgood Mountains, Humboldt County, Nevada: Unpublished Ph.D. dissertation, Stanford, California, Stanford University, 284 p.

Theodore, T.G., Silberman, M.L., and Blake, D.W., 1973, Geochemistry and K-Ar ages of plutonic rocks in the Battle Mountain mining district, Lander County, Nevada: U.S. Geological Survey Professional Paper 798-A, 24 p.

Wallace, A.R., 1993, Geologic map of the Snowstorm mountains and vicinity, Elko and Humboldt Counties, Nevada: U.S. Geological Survey Miscellaneous Investigation Series Map I-2394.

Wells, J.D., Stoiser, L.R., and Elliot, J.E., 1969, Geology and geochemistry of the Cortez gold deposit, Nevada: ECONOMIC GEOLOGY, v. 64, p. 526–537.

Wilson, P.N., and Parry, W.T., 1995, Characterization and dating of argillic alteration in the Mercur gold district, Utah: ECONOMIC GEOLOGY, v. 90, p. 1197–1216.

Wrucke, C.T., and Armubrustmacher, T.J., 1975, Geochemical and geologic relations of gold and other elements of the Gold Acres open pit mine, Lander County, Nevada: U.S. Geological Survey Professional Paper 860, 27 p.

York, D., 1969, Least squares fitting of a straight line with correlated errors: Earth and Planetary Science Letters, v. 5, p.320–324.